Early Earth's Phaneritic Ultramafic Rocks: Plate Tectonic Mantle Slices or Crustal Cumulates?

Jiawei Zuo[1,1,1], Alexander Webb[2,2,2], Emily Joyce Chin[3,3,3], Jason Harvey[4,4,4], Peter J Haproff[5,5,5], Thomas Mueller[6,6,6], Qin Wang[7,7,7], Lukáš Ackerman[8,8,8], Arthur H. Hickman[9,9,9], Dominik Sorger[10,10,10], and Anthony Ramírez-Salazar[11,11,11]

[1]The university of Hong kong
[2]University of Hong Kong
[3]Scripps Institution of Oceanography
[4]Leeds University
[5]University of North Carolina Wilmington
[6]Georg-August-Universität Göttingen
[7]Nanjing University
[8]Institute of Geology of the Czech Academy of Sciences
[9]Geological Survey of Western Australia
[10]Geoscience Center
[11]University of Leeds

November 30, 2022

Abstract

How and when plate tectonics initiated remain uncertain. In part, this is because many signals that have been interpreted as diagnostic of plate tectonics can be alternatively explained via hot stagnant-lid tectonics. One such signal involves early Archean phaneritic ultramafic rocks. In the Eoarchean Isua supracrustal belt of southwestern Greenland, some ultramafic rocks have been interpreted as mantle rocks tectonically exhumed during Eoarchean subduction. To explore whether all Archean phaneritic ultramafic rocks originated as cumulate and/or komatiite – i.e., without requiring plate tectonics – we examined the petrology and geochemistry of such rocks in the Isua supracrustal belt and the Paleoarchean East Pilbara Terrane of northwestern Australia, with Pilbara ultramafic rocks being representative of rocks from non-plate tectonic settings. We found that Pilbara ultramafic samples have cumulate textures and relative enrichment of whole-rock Os, Ir, and Ru versus Pt. In comparison, polygonal textures and variable whole-rock Os, Ir, Ru and Pt patterns are identified in Isua ultramafic samples. Isua and Pilbara ultramafic samples have (1) mineral assemblages that can form at crustal conditions; (2) broadly similar whole-rock major element patterns; (3) weakly fractionated to unfractionated trace element patterns that are close to primitive mantle values; and (4) spinel with variable TiO_2, relatively consistent Cr#, and variable and low Mg#. Many features of Isua or Pilbara ultramafic rocks are similar to depleted mantle rocks, except for spinel chemistry and cumulate textures. However, all features are consistent with cumulates. Collectively, these data permit [?]3.2 Ga initiation of plate tectonics on Earth.

Hosted file

`supplementary information.docx` available at https://authorea.com/users/558795/articles/607779-early-earth-s-phaneritic-ultramafic-rocks-plate-tectonic-mantle-slices-or-crustal-cumulates

Earth's earliest phaneritic ultramafic rocks 1: plate tectonic mantle slices or crustal cumulates?

Jiawei Zuo[1]*, A. Alexander G. Webb[1]*, Emily J. Chin[2], Lukáš Ackerman[3], Jason Harvey[4], Peter J. Haproff[5], Thomas Müller[6], Qin Wang[7], Arthur H. Hickman[8], Dominik Sorger[6], Anthony Ramírez-Salazar[4],

[1]Department of Earth Sciences and Laboratory for Space Research, University of Hong Kong, Pokfulam Road, Hong Kong, China

[2]Scripps Institution of Oceanography, University of California, San Diego, La Jolla, California 92093, USA

[3]Institute of Geology of the Czech Academy of Sciences, Rozvojová 269, Prague 6, 16500, Czech Republic

[4]School of Earth and Environment, University of Leeds, Leeds LS2 9JT, UK

[5]Department of Earth and Ocean Sciences, University of North Carolina Wilmington, North Carolina 28403, USA

[6]Geoscience Center, Department of Mineralogy, Georg-August-Universität Göttingen, D-37077 Göttingen, Germany

[7]State Key Laboratory for Mineral Deposits Research, School of Earth Sciences and Engineering, Nanjing University, Nanjing 210046, China

[8]Geological Survey of Western Australia, 100 Plain St., East Perth, Western Australia 6004, Australia.

*Corresponding authors: Jiawei Zuo (jwzuo@connect.hku.hk), Alexander Webb (aagwebb@hku.hk)

Key points:

1. Ultramafic rocks of the Isua supracrustal belt and the East Pilbara Terrane can be interpreted as crustal cumulates.
2. Isua and Pilbara ultramafic rocks interacted with co-existing low highly-siderophile-element lavas from deep, potentially reduced mantle and/or magma chambers
3. Isua ultramafic rocks do not represent plate tectonic mantle slices and do not require >3.7 Ga plate tectonics.

Abstract (300 words):

How and when plate tectonics initiated remain uncertain. In part, this is because many signals that have been interpreted as diagnostic of plate tectonics can be alternatively explained via hot stagnant-lid tectonics. One such signal involves early Archean phaneritic ultramafic rocks. In the Eoarchean Isua supracrustal belt of southwestern Greenland, some ultramafic rocks have been interpreted as tectonically-exhumed mantle during Eoarchean subduction. To explore whether all Archean phaneritic ultramafic rocks originated as cumulate and/or komatiite – i.e., without requiring plate tectonics – we examined the petrology and geochemistry of such rocks in the Isua supracrustal belt and the Paleoarchean East Pilbara Terrane of northwestern Australia, with Pilbara ultramafic rocks interpreted as representative of rocks from non-plate tectonic settings. We found that Pilbara ultramafic samples have relict cumulate textures, relative enrichment of whole-rock Os, Ir, and Ru versus Pt and Pd, and spinel with variable TiO_2, relatively consistent Cr#, and variable and low Mg#. Similar geochemical characteristics also occur in variably altered Isua ultramafic rocks. We show that Isua and Pilbara ultramafic rocks should have interacted with low Pt and Pd melts generated by sequestration of Pd and Pt into sulphide and/or alloy during magma generation or crystallization. Such melts cannot have interacted with a mantle wedge. Furthermore, altered mantle rocks and altered cumulates could have similar rock textures and whole-rock geochemistry such that they may not distinguish mantle from cumulate. Our findings suggest that depleted mantle interpretations are not consistent with geochemistry and/or rock textures obtained from Isua and Pilbara ultramafic rocks. Instead, cumulate textures of Pilbara samples, whole-rock Pt and Pd concentrations, and spinel geochemistry of Isua and Pilbara ultramafic rocks support cumulate origins and metasomatism involving co-genetic melts that formed in hot stagnant-lid settings. Collectively, these findings permit ≤ 3.2 Ga initiation of plate tectonics on Earth.

1. Introduction:

When, how, and why plate tectonics began on Earth remain among the most important unresolved questions in plate tectonic theory (e.g., Bauer et al., 2020; Beall et al., 2018; Brown and Johnson, 2018; Condie and Puetz, 2019; Hansen, 2007; Harrison, 2009; Korenaga, 2011; Nutman et al., 2020; Stern, 2008; Tang et al., 2020). Investigations of plate tectonic initiation have significant implications for questions associated with the evolution of early terrestrial planets, including whether early Earth experienced any pre-plate tectonic global geodynamics/cooling after the magma ocean stage (e.g., Bédard, 2018; Collins et al., 1998; Lenardic, 2018; Moore and Webb, 2013; O'Neill and Debaille, 2014); and why other terrestrial planets in the solar system appear to lack plate tectonic records (e.g., Moore et al., 2017; Stern et al., 2017; cf. Yin, 2012a; Yin, 2012b).

Many proposed signals for the initiation or early operation of plate tectonics on Earth are controversial due to the issue of non-uniqueness. For instance, the origin of Hadean zircons from the Jack Hills of western Australia has been contrastingly interpreted as (1) detrital crystals from felsic magmas generated by ~4.3 Ga plate subduction (Harrison, 2009; Hopkins et al., 2008); (2) zircons crystallized via impact heating and ejecta sheet burial (Marchi et al., 2014) or (3) low pressure melting of Hadean mafic crustal materials (Reimink et al., 2020). Similarly, researchers continue to debate whether the presence of Archean high Al_2O_3/TiO_2 mafic lavas (also known as boninite or boninitic basalts) must indicate subduction initiation as early as ~3.7 Ga (cf. Pearce and Reagan, 2019; Polat and Hofmann, 2003). Another example is how a ~3.2 Ga shift in zircon Hf-isotope signatures has been variably interpreted to indicate the onset of plate tectonics (Næraa et al., 2012) or enhanced mantle melting during a proposed mantle thermal peak (Kirkland et al., 2021). Due to these equivocal interpretations, the initiation of plate tectonics has been suggested to be ≤3.2 Ga using geological records that are generally considered unique to plate tectonics (e.g., paired metamorphic belts, ultra-high pressure [UHP] terranes, and passive margins) (e.g., Brown and Johnson, 2018; Cawood et al., 2018; Stern, 2008; cf. Bauer et al., 2020; Foley et al., 2014; Harrison, 2009; Korenaga, 2011; Nutman et al., 2020). The ≤3.2 Ga onset of plate tectonics requires early Earth tectonic evolution to be non-uniformitarian, involving some form of single-plate stagnant-lid tectonics (e.g., Bédard, 2018; Collins et al., 1998; Moore and Webb, 2013).

One proposed signal of early plate tectonics is the preservation of phaneritic ultramafic rocks in Eo- and Paleoarchean terranes. However, the issue of non-uniqueness also extends to their interpretations. In the Eoarchean Isua supracrustal belt and adjacent meta-tonalite bodies exposed in southwestern Greenland (**Fig. 1a**), some dunites and harzburgites have been interpreted to represent melt-depleted mantle rocks that experienced UHP metamorphism, percolated by arc basalts, and then emplaced on top of crustal rocks via subduction thrusting (e.g., Friend and Nutman, 2011; Nutman et al., 2020; Van de Löcht et al., 2018), similar to how modern ophiolitic ultramafic rocks formed in the mantle and are preserved in collisional massifs (e.g., Boudier et al., 1988; Lundeen, 1978; Wal and Vissers, 1993). These processes are not compatible with non-plate tectonic origins, where the ultramafic rocks can only be cumulates or high-Mg extrusive rocks (e.g., komatiites) without UHP metamorphic overprints and infiltration of arc lavas (Webb et al. 2020; Ramírez-Salazar et al. 2021). Although Szilas et al. (2015) and Waterton et al. (2022) argue that dunites and harzburgites in the Isua supracrustal belt can be interpreted as crustal cumulates formed by fractionation of Isua basalts, additional examinations are necessary to rule out depleted mantle origins of ultramafic protoliths, arc origins of associated melts, and thus plate tectonics as necessary for their igneous and metamorphic petrogenesis. Namely, further investigations of the igneous and metamorphic features of Isua ultramafic rocks, the origins of their potential parent melts, and the natures of melt/fluid components that have been interacted with them (Waterton et al., 2022; Friend and Nutman, 2011; Van de Löcht et al., 2020) are necessary outstanding tests. If Isua ultramafic rocks cannot be used as unequivocal indicators of plate tectonics, then the preservation of phaneritic ultramafic rocks in Eo- and Paleoarchean terranes may be all attributed to processes consistent with non-uniformitarian, non-plate tectonics.

This contribution explores the origins of Isua ultramafic rocks via analysis of new and published geochemical and petrological findings, including comparative analysis of key Isua samples and rocks of similar lithology from settings considered representative of hot stagnant-lid tectonics [In this study, we follow tectonic taxonomy from Lenardic (2018)]. The Paleoarchean geology of the East Pilbara Terrane of western Australia is widely accepted as representing hot stagnant-lid tectonics (Hickman, 2021; Johnson et al., 2014; Smithies et al., 2007, 2021; Van Kranendonk et al., 2004, 2007); Pilbara ultramafic samples are investigated in this study (**Fig. 1b**) as examples of ultramafic rocks from non-plate tectonic regimes. We also compare the petrology and geochemistry of Isua ultramafic rocks with those of (1) ultramafic cumulate rocks; (2) modelled ultramafic cumulate rocks; (3) melt-depleted mantle

rocks from plate tectonic settings; and (4) modelled melt-metasomatised depleted mantle rocks. We then derive possible petrogenetic models for both Isua and Pilbara ultramafic rocks, thereby examining whether the generation and alteration of these rocks are compatible with the predictions of hot stagnant-lid tectonics. Our findings help to evaluate whether plate tectonics is indeed required to explain the Eoarchean assembly of the Isua supracrustal belt. A complementary work (Müller et al., in prep.) further explores these tectonic questions via re-examination of the pressure-temperature conditions experienced by Isua ultramafic rocks.

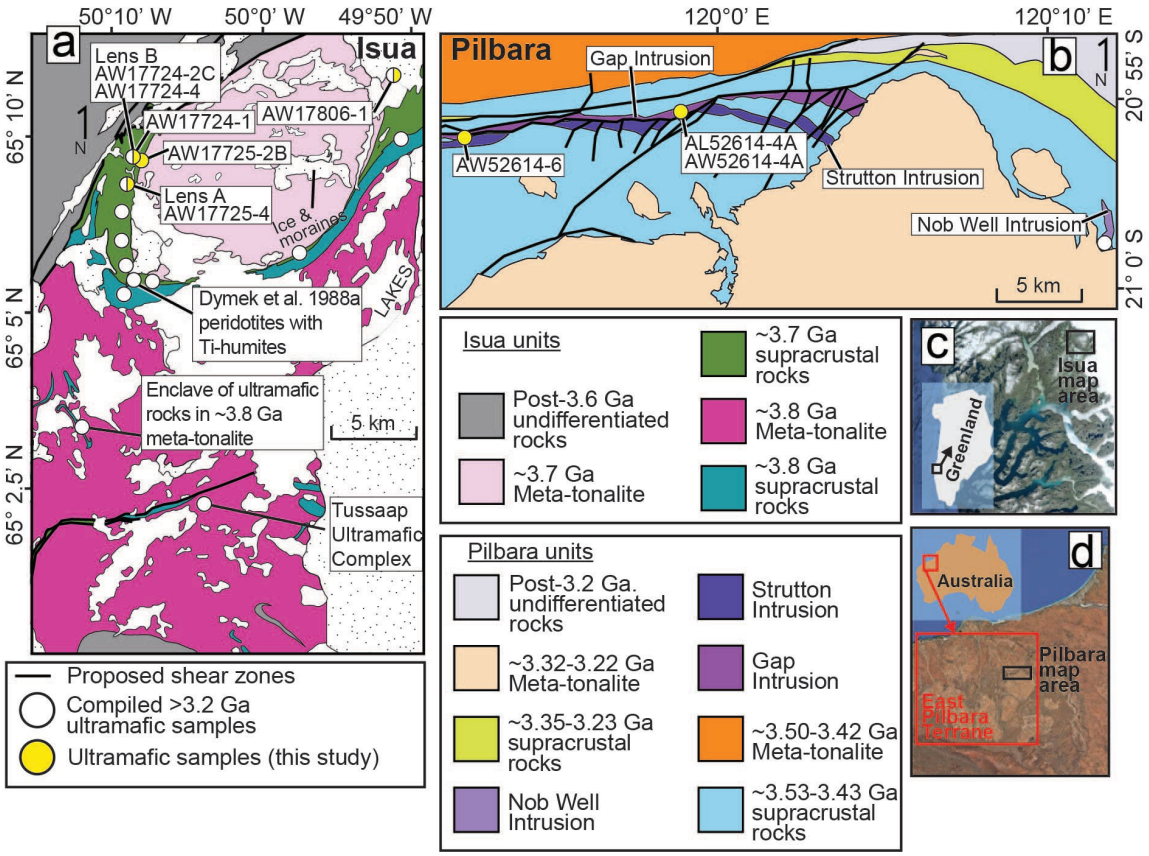

Figure 1. Geological maps of the Isua supracrustal belt, southwestern Greenland and north-central portion of the East Pilbara Terrane, northwestern Australia. **a**: simplified geology of the Isua supracrustal belt and adjacent areas [modified from Nutman et al. (2002)]. Locations of meta-peridotite enclaves and lenses A and B are presented. **b**: simplified geology of the north edge of the Mount Edgar Complex [modified from Van Kranendonk et al. (2007)] showing major km-scale ultramafic intrusive bodies: the Gap Intrusion, the Nob Webb Intrusion, and the Strutton Intrusion. **c:** location of the Isua supracrustal belt in southwestern Greenland. **d:** location of the East Pilbara Terrane in northwestern Australia. Yellow circles: locations for new samples; white circles, locations for compiled samples from Szilas et al. (2015), Van de Löcht et al. (2018), Friend et al. (2002), Friend and Nutman (2011), McIntyre et al. (2019), Dymek et al. (1988a), and the Geological Survey of Western Australia 2013 database.

2. Geological background and proposed tectonic models

2.1.The Isua supracrustal belt

The ~35-km-long, ~1–4 km-wide Isua supracrustal belt of southwestern Greenland is Earth's largest recognized Eoarchean terrane (**Fig. 1a**). The protoliths of the belt formed dominantly at ~3.8 Ga and ~3.7 Ga, and experienced extensive shearing, thinning, and folding (e.g., Nutman et al., 2020; Webb et al., 2020). Regional deformation of the Isua supracrustal belt is associated with amphibolite facies assemblages that have been interpreted to be Eoarchean (e.g., Nutman et al., 2020; Webb et al., 2020; Ramirez-Salazar et al., 2021; Zuo et al., 2021) and/or Neoarchean in age (e.g., Chadwick, 1990; Nutman, 1986; Nutman et al., 2015). Meta-tonalites of similar ages to the ~3.8 and 3.7 Ga supracrustal rocks are in contact with the Eoarchean supracrustal belt to the north and south (Crowley et al., 2002; Crowley, 2003). The interior of the belt exposes metamorphosed basalts (a high Al_2O_3/TiO_2 "boninitic" series and a low Al_2O_3/TiO_2 "tholeiitic" series, Szilas et al. 2015), chert, banded iron formation, and minor metamorphosed ultramafic igneous rocks, felsic volcanic rocks, and detrital sedimentary rocks (e.g., Nutman et al., 2002; Nutman and Friend, 2009).

Ultramafic rocks in the Isua area occur as ~1- to ~100-m-scale lenticular bodies associated with mafic pillow lavas (e.g., Dymek et al., 1988b; Szilas et al., 2015) and as enclaves in both north and south meta-tonalite bodies (e.g., Friend et al., 2002; Nutman and Friend, 2009). These ultramafic rocks appear to have experienced various degrees of alteration including carbonitization and serpentinization (e.g., Dymek et al., 1988b; Friend et al., 2002; Szilas et al., 2015). Two ~10^4 m^2 meta-peridotite lenses (lens A in the south and lens B in the north) located ~1.5-km apart along the eastern edge of the western Isua supracrustal belt and some ultramafic enclaves (as large as ~10^4 m^2) in meta-tonalite located ~15 km south of the belt (**Fig. 1a**) contain dunites and/or harzburgites with relatively weak carbonitization and serpentinization (e.g., Friend et al. 2002; Friend and Nutman, 2011; Nutman and Friend, 2009; Szilas et al., 2015). Igneous, metamorphic and deformation features of these dunites and harzburgites have been explored to constrain the Eoarchean tectonic evolution of the Isua supracrustal belt (e.g., Kaczmarek et al., 2016; Nutman et al., 2020; Van de Löcht et al., 2018; Guotana et al., 2022; Waterton et al. 2022). These include: (1) primary rock textures and deformation overprints, such as polygonal textures and B-type olivine deformation

fabrics observed in dunites from the meta-peridotite lenses A and B in the Isua supracrustal belt (Kaczmarek et al., 2016; Nutman et al., 1996); (2) a mineral assemblage of olivine + serpentine ± pyroxene ± Ti-humite ± carbonate ± spinel ± ilmenite ± magnesite for dunites from lenses A and B (e.g., Guotana et al., 2022; Nutman et al., 2020; Szilas et al., 2015) and a mineral assemblage of olivine + serpentine + pyroxene + spinel ± hornblende for meta-peridotites from the ultramafic enclaves (Van de Löcht et al., 2018, 2020); (3) primitive mantle-normalized rare earth element patterns (REE) that are sub-parallel to those of nearby basalts (e.g., Szilas et al., 2015; Van de Löcht et al., 2020) or komatiite (Dymek et al., 1988b); and (4) various highly siderophile element (HSE) patterns, including relatively high primitive mantle-normalized Os, Ir and Ru versus Pt and Pd preserved in ultramafic enclaves in the south meta-tonalite (Van de Löcht et al., 2018), and similar patterns preserved in the two meta-peridotite lenses of the Isua supracrustal belt (Waterton et al. 2022).

The Isua supracrustal belt has been mostly interpreted to record ~3.8–3.6 Ga plate tectonic processes, including subduction and subsequent extension (e.g., Arai et al., 2015; Nutman et al., 2020; Nutman et al., 2013b; Nutman and Friend, 2009). The presence of dunites in meta-peridotite lenses A and B has been used to support such a plate tectonic origin (e.g., Friend and Nutman, 2011; Nutman et al., 2020; Van de Löcht et al., 2020) as these dunites were interpreted as highly depleted mantle residues tectonically thrust atop of supracrustal rocks in an Eoarchean subduction setting (see Figure 8 of Nutman et al., 2013a). In this context, Isua dunites were interpreted as initially melt-depleted olivine ± pyroxene ± spinel mantle residues. These residues experienced fluid- and/or rock-dominated serpentinization, and UHP metamorphism, as well as melt percolation in an Eoarchean mantle wedge, such that Isua dunites preserve Ti-humite, variably fractionated HSE patterns, REE patterns parallel to those of nearby basalts, and/or olivine with clinopyroxene inclusions and mantle-like oxygen isotopes (e.g., Friend and Nutman, 2011; Nutman et al., 2020, 2021a). Olivine B-type fabrics were interpreted as recording deformation in the mantle wedge (Kaczmerak et al., 2016). The deformed and variably altered sub-arc mantle residues were then juxtaposed with Isua supracrustal rocks via thrusting in an Eoarchean suprasubduction zone (e.g., Nutman et al., 2020) and experienced additional modification during and after Eoarchean (e.g., Nutman et al., 2021a; Guotana et al. 2022).

Recently, a heat-pipe model (i.e., a subcategory of hot stagnant-lid tectonics) was proposed as an alternative to plate tectonics for the formation and deformation of the Isua supracrustal belt (Webb et al., 2020). Like other hot stagnant-lid tectonic models (e.g.,

Collins et al., 1998; Johnson et al., 2014), heat-pipe tectonics is dominated by (sub-)vertical transport of materials, but the main driving force of this transport is volcanic advection rather than gravitational instability (Moore and Webb, 2013; O'Reilly and Davies, 1981). Voluminous mafic volcanism causes heat to be lost to the atmosphere/space, and extensive volcanic depositional resurfacing as well as burial and downwards advection of cold surface materials. The volume loss from the ascent of hot magmatic materials is ultimately balanced by the descent of the cold volcanic materials. At great depths, portions of buried hydrated mafic crust are partially melted, forming tonalitic melts. Other lower crustal rocks (along with varying fractions of their fluid components) are recycled into the convecting mantle. Therefore, in contrast to the idea that hot stagnant-lid regimes should lack material exchange between surface and mantle (e.g., Nutman et al. 2021b), volcanic advection in a heat-pipe setting is an efficient mechanism to generate crust recycling and fluid-fluxing between crust and mantle (e.g., Moore and Webb, 2013; O'Reilly and Davies, 1981). Crustal deformation of a heat-pipe lithosphere is predicted to happen via (1) radial shortening due to subsidence of crustal materials in Earth's quasi-spherical geometry (Bland and McKinnon, 2016; Moore and Webb, 2013); or (2) contraction during a plate-breaking and subduction event as or soon after the heat-pipe cooling ceases (Beall et al., 2018; Moore and Webb, 2013; Tang et al. 2020). Alternatively, deformation of a preserved fragment of heat-pipe lithosphere may be possible at any subsequent time when involved in a deformation zone of any tectonic setting. With respect to the formation of ultramafic rocks, this model does not involve the thrusting of mantle rocks atop crustal rocks, given that subduction and associated mantle wedge settings do not occur during heat-pipe cooling. Therefore, the heat-pipe model requires all Isua ultramafic rocks to represent high MgO lavas (e.g., komatiites) or cumulates formed in magma chambers. In this context, the geochemical signatures of Isua ultramafic rocks were controlled by parental melt compositions, fractional crystallization, melt-cumulate mixing and re-equilibration, and/or fluids/materials released from crustal rocks. Their rock textures were produced by crystallization of melts and/or subsequent deformation/mineral re-equilibration under crustal conditions. Metamorphic assemblages observed in Isua ultramafic rocks were formed under amphibolite facies conditions, consistent with other parts of the belt (e.g., Ramírez-Salazar et al., 2021; Müller et al., in prep.; cf. Friend and Nutman, 2011; Nutman et al. 2020).

2.2.The East Pilbara Terrane

The ~40,000 km^2 East Pilbara Terrane of northwestern Australia is Earth's largest and best-preserved Paleoarchean terrane (**Fig. 1b**). There, eleven granitoid bodies (mostly meta-tonalites, with minor granites) are surrounded by broadly coeval supracrustal belts. These supracrustal belts are dominantly comprised of metamorphosed mafic to felsic volcanic rocks, with some chemical and clastic sedimentary rocks, and layered ultramafic rocks and intrusions (e.g., Van Kranendonk et al., 2007; Hickman, 2021). Rock formation, deformation, and metamorphism (largely greenschist facies) in the East Pilbara Terrane are thought to have mostly occurred from ~3.5–3.2 Ga, such that by the end of the Paleoarchean, the supracrustal belts had been deformed into synforms and the granitoids had become domes (Collins et al., 1998; Van Kranendonk et al., 2007). This regional "dome-and-keel" geometry is a key element for tectonic interpretations of the East Pilbara Terrane (described below).

Ultramafic rocks of the East Pilbara Terrane occur as layers or pods interleaved with supracrustal rocks and as km-scale igneous bodies intruding supracrustal sequences (e.g., Smithies et al., 2007). Ultramafic layers and pods found in the supracrustal sequences commonly have thicknesses of ~1–5 meters and, preserve spinifex textures in some locations. These rocks have been interpreted to have been crystallized from komatiitic or basaltic lava flows (e.g., Smithies et al., 2007; Van Kranendonk et al., 2007). In this study, we focus on the km-scale intrusions. The East Pilbara Terrane exposes three >10-km-long and >100-m-thick ultramafic intrusive bodies (**Fig. 1b**), which include the Gap Intrusion, the Strutton Intrusion, and the Nob Well Intrusion. These ultramafic bodies intrude ~3.53–3.43 Ga supracrustal sequences and are intruded themselves by ~3.31 Ga granodiorites (**Fig. 1b**) (Williams, 1999). Existing knowledge of these ultramafic rocks is mostly limited to map relationships, petrological descriptions and geochemical data published by the Geological Survey of Western Australia (e.g., Williams, 1999). In general, these ultramafic intrusions are comprised of variably metamorphosed peridotite (including dunite), pyroxenite, and gabbro (Geological Survey of Western Australia 2013 database).

Most researchers interpret that East Pilbara Terrane represents a Paleoarchean terrane formed via regional hot stagnant-lid tectonics that featured vigorous (ultra)mafic and felsic volcanism (e.g., Collins et al., 1998; Johnson et al., 2017; François et al., 2014; Moore and Webb, 2013; Van Kranendonk et al., 2007; Van Kranendonk, 2010; Wiemer et al., 2018) although a plate tectonic origin has also been proposed (e.g., Kusky et al., 2021). One subcategory of this tectonic regime is the partial convective overturn cooling model (Collins et al., 1998), which predicts that the East Pilbara Terrane experienced episodic supracrustal

volcanism and tonalite formation followed by quiescence during ~10 to ~100 million years cycles of mantle plume activities. In this model, (ultra)mafic magmatism associated with mantle plumes produces km-scale ultramafic intrusions with or without fractional crystallization (e.g., Smithies, 2007). The partial convective overturn cooling model involves gravitational instability between the relatively hot, buoyant tonalite bodies and colder, denser supracrustal materials. Such instability could lead to diapiric rise of tonalites and folding of supracrustal rocks deformed into synclines surrounding the tonalite domes, creating the observed "dome-and-keel" geometry. No subduction activity and associated mantle-derived ultramafic rocks are predicted at the crustal levels of a partial convective overturn lithosphere (e.g., Collins et al., 1998). Indeed, no lithology so far in the East Pilbara Terrane has been interpreted as tectonically emplaced mantle rocks (Hickman et al., 2021). Thus, Pilbara ultramafic rocks can be used as non-plate tectonic crustal products to compare with Isua ultramafic rocks.

3. Methods:

Three ultramafic samples (AL52614-4A, AW52614-4A, and AW52614-6) collected from the Gap Intrusion of the East Pilbara Terrane and six samples (AW17724-1, AW17724-2C, AW17724-4, AW17725-2B, AW17725-4 and AW17806-1) collected from the Isua supracrustal belt were analyzed in this study (**Fig. 1**). Isua samples AW17724-2C, AW17724-4 (lens B in the north) and AW17725-4 (lens A in the south) were collected from the two meta-peridotite lenses which have been previously interpreted as tectonic mantle slices (e.g., Friend and Nutman, 2011; Nutman et al., 2020)]. Isua sample AW17724-1 was collected from the serpentinite layer enveloping the meta-peridotite lens B. Isua sample AW17725-2B was collected from an ultramafic outcrop near the northern meta-tonalite, ~300 meters east of the lens B. Isua sample AW17806-1 was collected from an outcrop located at the eastern supracrustal belt near the northern meta-tonalite body (**Fig. 1a, Table 1**).

To test models of their petrogenesis, we compiled literature data and inspected our samples using thin-section petrography and acquisition of (1) whole-rock major/trace element data (Table S1); (2) spinel geochemistry (Table S2); and (3) HSE abundances (Table S3). Compiled Isua and Pilbara data include results of previous studies focused on ultramafic rocks located adjacent to our sample locations. These outcrops specifically include (1) ultramafic rocks collected across the Isua supracrustal belt (including the meta-peridotite lenses) studied by Szilas et al. (2015), Friend and Nutman (2011) and Waterton et al. (2022)

(**Fig. 1a**); (2) ultramafic rocks from the enclaves within the meta-tonalite located south of the Isua supracrustal belt (Van de Löcht et al., 2018, 2020); and (3) ultramafic rocks from the Nob Well Intrusion of the East Pilbara Terrane (Geological Survey of Australia 2013 database; **Fig. 1b**). Data from other ultramafic rocks that have been variably interpreted as cumulates or mantle peridotites (see Figures 3–8 captions for all references) are compiled for comparison with the ultramafic lithologies of this study. These rocks were collected from variably deformed and altered Archean ultramafic complexes (e.g., McIntyre et al., 2019), massive layered intrusions (e.g., Coggon et al., 2015), collisional massifs (e.g., Wang et al., 2013), volcanic xenoliths (e.g., Ionov, 2010) or mantle rocks extracted from ocean drilling (e.g., Parkinson and Pearce, 2008). Modelled cumulates (Mallik et al. 2020) and variably depleted and refertilized mantle rocks (e.g., Chin et al. 2014, 2018) are also generated (see section 5.3) or compiled for comparison.

3.1. Analytical details

The whole-rock major element concentrations of Pilbara ultramafic samples were analyzed in the Peter Hooper GeoAnalytical Laboratory at Washington State University. Major elements (e.g. MgO, FeOt, and SiO_2) were analyzed using a Thermo-ARL Advant'XP+ sequential X-ray fluorescence spectrometer (XRF). Sample preparation, analytical conditions, and precisions/accuracy of the analyses follow procedures detailed in Johnson et al. (1999). The whole-rock major element concentrations of Isua ultramafic samples were determined at the State Key Laboratory for Mineral Deposit Research in Nanjing University, China. Small fresh rock fragments of Isua ultramafic samples were firstly crushed into gravel-size chips. Clean chips were then powdered to 200 mesh for major element analysis. Measurements of whole-rock major elements were performed by using a Thermo Scientific ARL 9900 XRF. The measured values of diverse rock reference materials (BHVO-2 and BCR-2) indicate that the uncertainties are less than ±3% for elements Si, Ti, Al, Fe, Mn, Mg, Ca, K and P and less than ±6% for Na.

Trace element concentrations of Pilbara ultramafic samples were acquired using an Agilent 7700 inductively coupled plasma mass spectrometer (ICP-MS) in the Peter Hooper GeoAnalytical Laboratory at Washington State University. Sample preparation, analytical conditions, and precisions/accuracy of the analyses can be found in detail in Knaack et al. (1994). Trace element contents of Isua ultramafic samples were obtained at Nanjing Hongchuang Exploration Technology Service Co., China. About 100 grams of solid samples

from each Isua ultramafic sample were first crushed into smaller grains with a corundum jaw crusher. They were then crushed into fine powder using an agate ball mill. Details of sample preparation, analytical procedures, and precisions are as follows. The digestion method of silicate rock samples is closed pressure acid dissolution method. The specific steps are as follows: 50 mg of rock powder were weighed directly into a steel-jacketed high-pressure polytetra fluoroethylene bomb and then dissolved using an acid mixture of 1.5 mL of 29 mol/L HF and 1 mL of 15 mol/L HNO_3 at 190 °C for 72 hours. Then, the digested solution was evaporated to wet salt and treated twice with 1 mL of concentrated HNO_3 to avoid the formation of fluorides. Finally, the evaporated residue was dissolved with 1.5 mL HNO_3 and 2 mL H_2O and the Teflon bomb was resealed and placed in the oven at 190 °C for 12 hours. The final solution was transferred to a polyethylene bottle and diluted to 50 mL using H_2O. Trace element analyses were performed on an Agilent 7900 inductively coupled plasma mass spectrometry (ICP-MS). The total quantitative analyses of trace elements were achieved by external standard BCR-2 and BHVO-2 and internal standard Rh dopped on line using an Agilent 7900 ICP-MS wet plasma. All elements are repeatedly scanned for five times, which precision 1RSD are better than 5 %. The margin of error of all trace element results for rock powder reference materials was guaranteed to be plus or minus within 10 %.

The major element compositions of spinel from the Pilbara ultramafic samples were obtained using a JEOL JXA8230 Electron Probe Microanalyser (EMPA) at the University of Leeds, United Kingdom. Major element mineral (e.g., olivine, spinel, and serpentine) compositions of the Isua ultramafic samples were analyzed in situ on petrographic thin sections by a JEOL JX8100 Electron Probe Microanalyser at the Guangzhou Institute of Geochemistry, Chinese Academy of Sciences. At the Guangzhou facility, a Carl Zeiss SUPRA55SAPPHIR Field Emission Scanning Electron Microscope was used to collect images of the Isua ultramafic samples.

The HSE concentrations and Re–Os isotopic data were obtained at the Institute of Geology of the Czech Academy of Sciences, Czech Republic, using the methods detailed in Topuz et al. (2018). In brief, the samples were dissolved and equilibrated with mixed ^{185}Re-^{190}Os and ^{191}Ir–^{99}Ru–^{105}Pd–^{194}Pt spikes using Carius Tubes (Shirey and Walker, 1995) and reverse aqua regia (9 ml) for at least 72 hours. Decomposition was followed by Os separation through solvent extraction by $CHCl_3$ (Cohen and Waters, 1996) and Os microdistillation (Birck et al., 1997). Iridium, Ru, Pt, Pd, and Re were separated from the remaining solution using anion exchange chromatography and then analyzed using a sector field ICP-MS

Element 2 (Thermo) coupled with Aridus II^{TM} (CETAC) desolvating nebulizer. The isotopic fractionation was corrected using a linear law and standard Ir, Ru, Pd, Pt (E-pond), and Re (NIST 3143) solutions that were run with samples. In-run precision of measured isotopic ratios was always better than ±0.4% (2 σ). Os concentrations and isotopic ratios were obtained using negative thermal ionization mass spectrometry (Creaser et al., 1991; Völkening et al., 1991). Samples were loaded with concentrated HBr onto Pt filaments with $Ba(OH)_2$ activator and analyzed as OsO_3^- using a Thermo Triton thermal ionization spectrometer with Faraday cups in dynamic mode, or using a secondary electron multiplier in a peak hopping mode for samples with low Os concentrations. Internal precision for $^{187}Os/^{188}Os$ determination was always equal to or better than ±0.2% (2 σ). The measured Os isotopic ratios were corrected offline for oxygen isobaric interferences, spike contribution and instrumental mass fractionation using $^{192}Os/^{188}Os = 3.08271$ (Shirey and Walker, 1998).

Literature data of Isua ultramafic rocks, crustal cumulates, and mantle peridotites are compiled for comparison (see figure captions for data sources). Fe contents of all complied data were recalculated to represent FeOt using the procedure in Gale et al. (2013). Results were plotted with GCDKit freeware developed by Janoušek et al. (2006).

4. Results

4.1. Petrographic observations

We performed thin-section petrographic analysis of both Isua and Pilbara ultramafic samples to observe rock microtextures and mineral assemblages that reflect igneous and alteration signatures, as these are important for the interpretation of geochemistry of altered samples. Isua ultramafic samples show varying degrees of alteration (**Fig. 2, Fig. S1**). Samples AW17724-1, AW17724-4, and AW17725-2B are dominated by serpentine, magnetite and carbonates with the absence of olivine, pyroxene, or protolith textures (**Fig. 2d, Fig. S1**). On the other hand, olivine grains are preserved in three samples (i.e., AW17724-2C from lens B, AW17725-4 from lens B and AW17806-1; **Fig. 2a**–**c**), where they are cross-cut or overgrown by retrograde serpentine minerals (**Fig. 2a**). In addition to serpentinization, meta-peridotite lens samples AW17724-4C and AW17725-4 show varying degrees of carbonitization (**Fig. 2a–b**), whereas sample AW17806-1 records tremolite as an alteration product (**Fig. 2c**). Small (submicron to ~20 μm) serpentine, magnesite, and/or magnetite can be found within olivine grains as inclusions or alteration products associated with cracks/veins not visible on the thin section planes (**Fig. 2a–b**). Relict olivine grains

407 preserved in sample AW17725-4 show polygonal textures, but the protolith textures of
408 AW17806-1 and AW17724-2C are altered beyond recognition (**Fig. 2b–c)**. Ti-humite phases
409 only occur in AW17724-4 (**Fig. 2a**; see Müller et al., in prep. for detailed petrological
410 observations for this sample).

411 In contrast to Isua samples, Pilbara samples have experienced complete serpentinization
412 and minor carbonitization, such that no primary ferromagnesian silicates can be identified
413 (**Fig. 3a–c, Fig. S1**). In all Pilbara samples, serpentine grains form clusters that show similar
414 extinction. Many such clusters have quasi-equant granular outlines. We interpret these
415 serpentine clusters to be pseudomorphs after olivine. The interstitial space between the
416 olivine-shaped clusters is occupied by chlorite and/or Fe-Cr-Ti oxide minerals (**Fig. 3a–b**) or
417 serpentine (**Fig. 3a–c**). The olivine-shaped serpentine clusters appear to form self-supporting
418 structures. Some interstitial serpentine clusters appear to preserve two pairs of relict
419 cleavages at ~90°, indicating a pyroxene precursor (**Fig. 3a**). Some interstitial serpentine
420 clusters are larger than the olivine-shaped serpentine clusters and enclose many of the latter
421 grains (illustrated in **Fig. 3c**: two sets of serpentine clusters can be recognized via different
422 brightness due to extinction). Such patterns resemble poikilitic textures in which early-
423 formed chadacrysts are surrounded by younger, large oikocrysts (Johannsen, 1931). In some
424 locations, the olivine-shaped serpentine clusters are compacted, forming polygonal textures
425 (**Fig. 3c**). Late-stage alterations veins/cracks can be seen in samples AW52514-4A and
426 AL52614-4A (**Fig. 3b**).

427

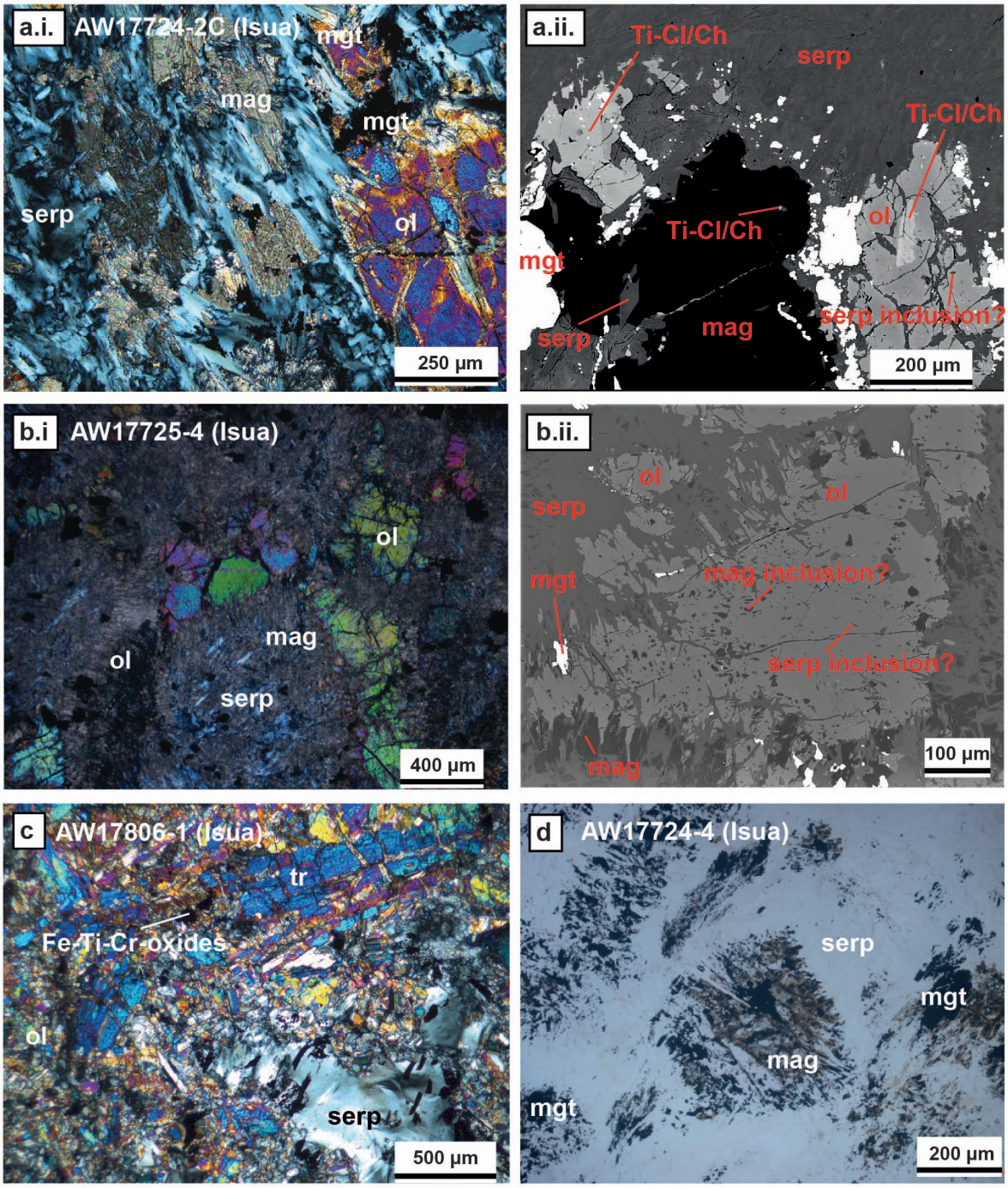

Figure 2. Representative thin section microphotographs and scanning electron microscopic images of samples from the Isua supracrustal belt. **a:** Sample AW17724-2C preserves primary olivine grains (**i** and **ii**). There may be two generations of serpentine minerals (**ii**): serpentine minerals that might be inclusions in the olivine grains, and serpentine minerals occur as lepidoblastic assemblages in the matrix cutting olivine, magnesite, and Ti-humite. Alternatively, there may be only one generation of serpentine minerals with those in the olivine being associated with cracks or veins not visible on this thin section plane. Due to the observed alteration, primary igneous textures of this sample

cannot be identified. **b:** Local preservation of polygonal textures (**i**) by olivine grains in sample AW17725-4. Olivine in this sample contains abundant magnesite and rare serpentine (**ii**), which may represent inclusions or alteration products. **c–d:** Loss of most primary ultramafic silicates and rock textures of some Isua samples due to strong alteration (e.g., serpentinization and/or amphibolite facies metamorphism). Mineral abbreviations: mag: magnesite; mgt: magnetite; ol: olivine; serp: serpentine; Ti-cl: Titano-clinohumite; Ti-ch: Titano-chondrodite; tr: tremolite.

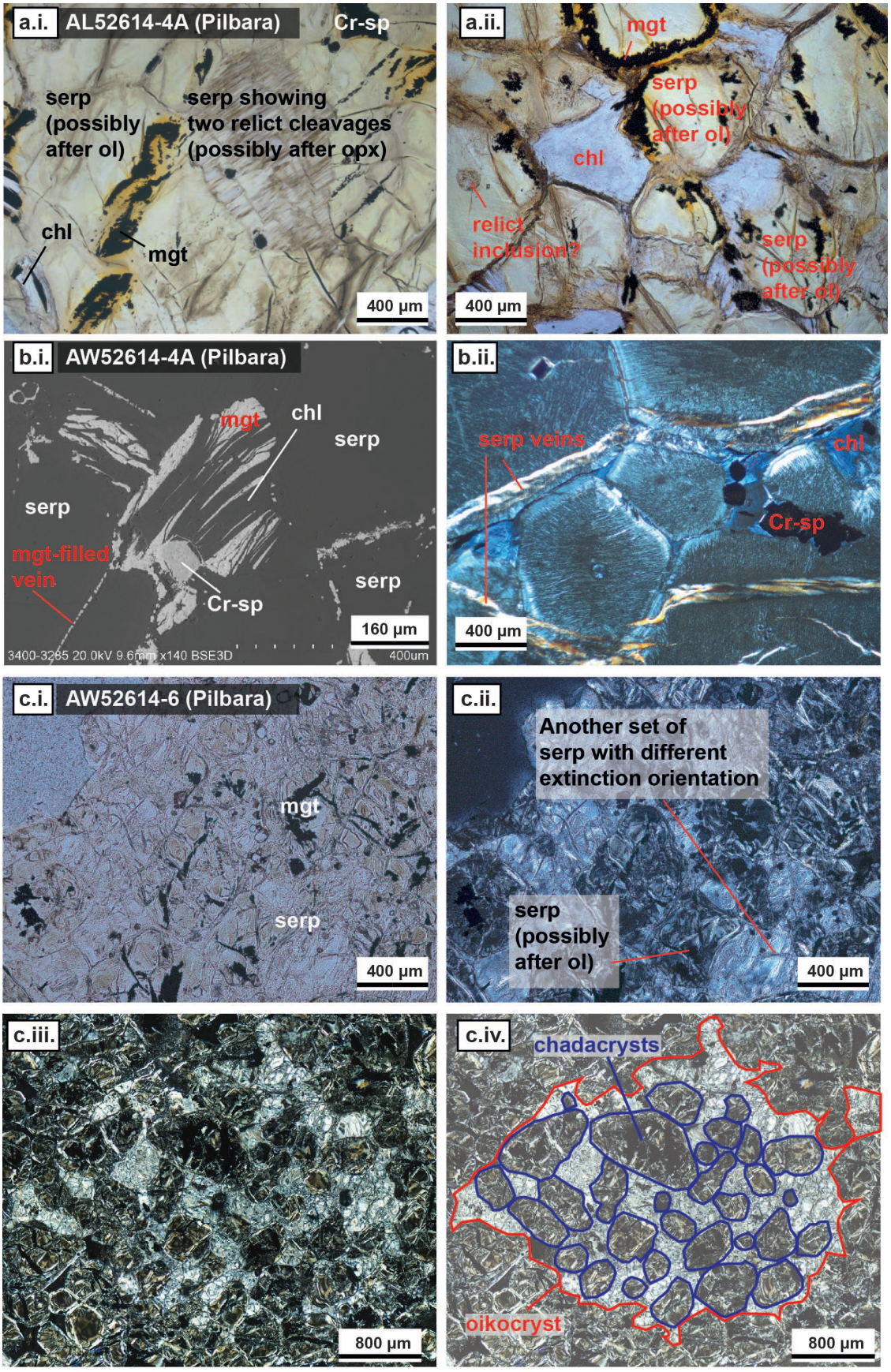
a.i.
AL52614-4A (Pilbara)
Cr-sp
serp (possibly after ol)
serp showing two relict cleavages (possibly after opx)
chl
mgt
400 µm
a.ii.
mgt
serp (possibly after ol)
chl
relict inclusion?
serp (possibly after ol)
400 µm
b.i.
AW52614-4A (Pilbara)
mgt
chl
serp
serp
mgt-filled vein
Cr-sp
serp
160 µm
3400-3265 20.0kV 9.6mm x140 BSE3D
400um
b.ii.
serp veins
chl
Cr-sp
400 µm
c.i.
AW52614-6 (Pilbara)
mgt
serp
400 µm
c.ii.
Another set of serp with different extinction orientation
serp (possibly after ol)
400 µm
c.iii.
800 µm
c.iv.
chadacrysts
oikocryst
800 µm

448

449

Figure 3. Representative thin section microphotographs and scanning electron microscopic images of samples from the East Pilbara Terrane. Pilbara samples show complete serpentinization, yet their primary rock textures are preserved by serpentine pseudomorphs. **a:** Sample AW52614-4A shows compacted olivine-shaped serpentine clusters (**ii**) which locally form polygonal textures (featured by abundant 120° triple junctions). **b:** Alteration minerals such as chlorite, serpentine and magnetite occur in interstitial spaces **(i)** and veins in sample AW52614-4A **(ii)**. In **c.ii**, **c.iii** and **c.iv**, two sets of serpentine clusters are recognized with the cross-polarized light photomicrographs. One set shows black/dark grey color, with outlines similar to olivine grains. Another set is in white/light grey, which appears to enclose the serpentine clusters of the first set. This texture resembles cumulate textures, where smaller chadacrysts could be included in larger oikocrysts. Mineral abbreviations: chl: chlorite; Cr-sp: Cr-spinel; mag: magnesite; mgt: magnetite; ol: olivine; opx: orthopyroxene; serp: serpentine;

Table 1: Mineralogy and location information of investigated samples.

Sample ID	GPS coordinates (WGS84 datum)	Location/Unit	Mineralogy
The Isua supracrustal belt			
AW17724-1	65.153681 N, 50.143989 W	Serpentinite layer enveloping the meta-peridotite lens B in the western belt	serpentine+talc+magnetite
AW17724-2C	65.153974 N, 50.144801 W	The meta-peridotite lens B in the western belt	olivine+serpentine+magnetite±Ti-humite±magnesite
AW17724-4	65.156859 N, 50.143249 W	The meta-peridotite lens B in the western belt	serpentine+magnetite+magnesite±talc
AW17725-2B	65.154857 N, 50.138543 W	~300 meters east of lens B in the western belt	carbonate+magnetite±serpentine
AW17725-4	65.139544 N, 50.149716 W	The meta-peridotite lens A in the western belt	serpentine+magnesite+olivine±magnetite
AW17806-1	65.191627 N, 49.840547 W	An outcrop in the eastern belt near the north tonalite	olivine+pyroxene+tremolite ±serpentine±Fe-Ti-Cr oxides
The East Pilbara Terrane			
AW52614-4A	20.917983 S, 119.982300 E	The Gap Intrusion	serpentine+Fe-Ti-Cr oxides+chlorite±apatite
AL52614-4A	20.917983 S, 119.982300 E	The Gap Intrusion	serpentine+Fe-Ti-Cr oxides+chlorite
AW52614-6	20.930950 S, 119.867500 E	The Gap Intrusion	serpentine+Fe-Ti-Cr oxides+chlorite

4.2.Whole-rock major and trace element characteristics

Whole-rock major and trace element characteristics are often used to indicate the petrogenetic conditions, such as the degree of melt depletion, and the sources of ultramafic rocks (e.g., Niu and Hekinian, 1997; Van de Löcht et al., 2020), although effects of alteration (as observed in section 4.1) must be considered. Isua ultramafic rocks have SiO_2 of ~38–49

wt.%, MgO of ~31–47 wt.%, CaO of ~0.03–10.49 wt.%, Al_2O_3 of ~0.5–5.0 wt.%, FeOt of ~6.2–10.7 wt.%, Mg# [i.e., Mg/(Mg+Fe)] of 84–93, and loss-on-ignition (LOI) of ~5–21 wt.% (all major oxide concentrations are anhydrous values, i.e., normalized to zero LOI and 100 wt.% total; **Figs. 4–6, Table S1**). The trace element abundances of Isua ultramafic samples are mostly 0.1–10 times to those inferred for the primitive mantle (McDonough and Sun, 1995; same below; **Fig. 7**). These samples show an unfractionated to mildly fractionated trend from light to medium rare earth elements (LREE to MREE) with $(La/Sm)_{PM}$ values ranging from ~1.1–3.8 (**Fig. 7a, 7c**). The heavy rare earth elements (HREE) of Isua ultramafic samples indicate a flat trend or variably fractionated trends with $(Gd/Yb)_{PM}$ of ~0.3–1.6 (**Fig. 7a**). The Th concentrations and Gd/Yb ratios (proxies for alterations; **Fig. 7b**; Deschamps et al., 2013) of Isua ultramafic samples range from 0.04–1.13 ppm and 0.4–2.1, respectively. Some Isua ultramafic samples show negative Nb anomalies. Positive or negative Eu anomalies can both be identified in Isua ultramafic samples (**Fig. 7c**).

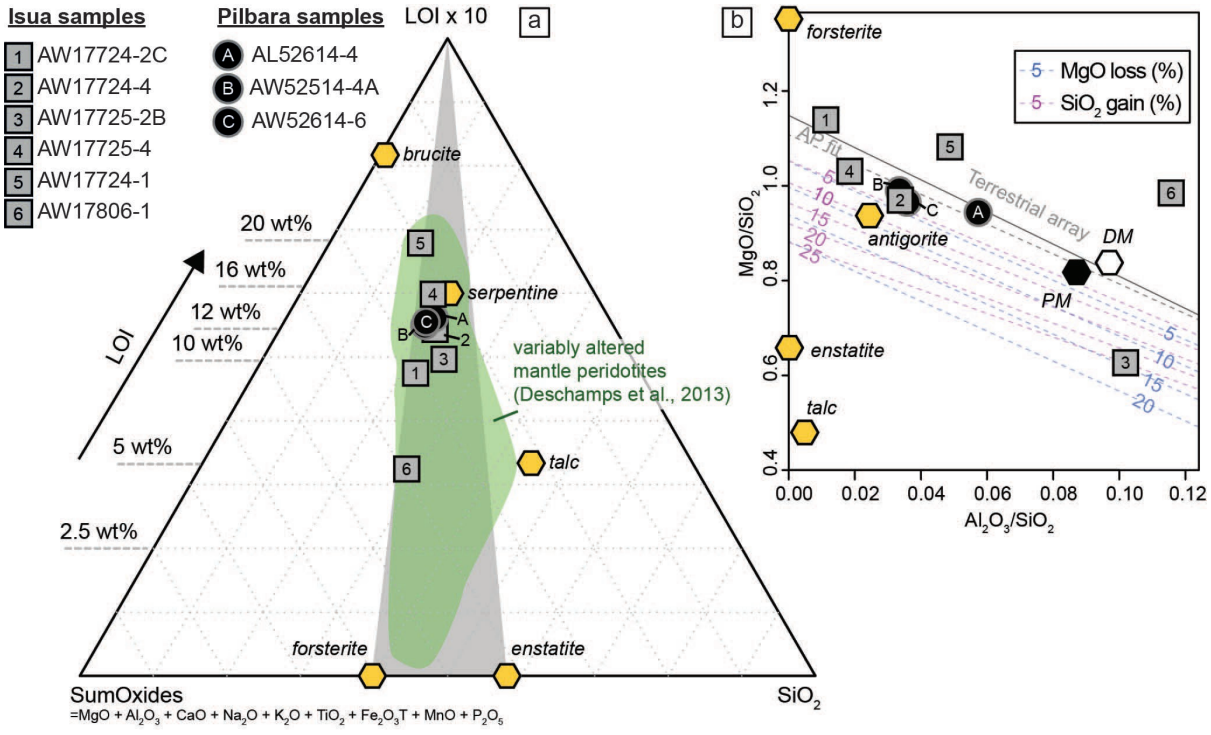

Figure 4. Major element and loss-on-ignition (LOI) geochemical characteristics of Pilbara and Isua ultramafic samples in comparison with common primary and alteration minerals in ultramafic rocks. All major element concentrations are anhydrous values (i.e., normalized to zero LOI and 100 wt.% total). Panel **a** shows a ternary plot of SiO_2, LOI, and SumOxides ($MgO + Al_2O_3 + CaO + Na_2O + K_2O + TiO_2 + Fe_2O_3T + MnO + P_2O_5$) (modified from Deschamps et al., 2013).

Panel **b** shows MgO/SiO_2–Al_2O_3/SiO_2 space with Pilbara and Isua ultramafic samples, common primary and alteration minerals in ultramafic rocks, the terrestrial array of mantle peridotites (fitted by abyssal peridotites, AP), and MgO-loss or SiO_2-gain alteration curves. The data in this figure show that the major element systematics of our Isua and Pilbara samples reflect various degrees of serpentinization without strong talc alteration, consistent with thin-section petrography (**Figs. 2–3**). Two samples (AW17725-2B, AW17806-1) which were collected from outcrops near the meta-tonalite have significantly elevated Al_2O_3. These high Al concentrations cannot be attributed to serpentinization and talc alteration. Panel b is modified from Malvoisin et al. (2015) which itself is a modified version of Jagoutz (1979). PM: primitive mantle; DM: depleted mantle. All mantle values are from McDonough and Sun (1995).

Pilbara ultramafic rocks have whole-rock SiO_2 of ~43–46 wt.%, MgO of ~41–45 wt.%, CaO of 0.02–0.12 wt.%, Al_2O_3 of ~1.6–2.5 wt.%, FeOt of ~6.1–12.8 wt.%, Mg# of 85–93, and LOI of 12.3–12.9 wt.% (**Figs. 4–6, Table S1**)**.** The trace element abundances in these samples are also 0.1–10 times to those of primitive mantle. Pilbara samples show fractionated LREE to HREE, with $(La/Sm)_{PM}$ ranging from 1.9 to 2.4 (**Fig. 7**). These samples have weak negative Nb anomalies, negative Eu anomalies, and generally flat HREE trends [with $(Gd/Yb)_{PM}$ of 0.8–1.1]. The Th concentrations and Gd/Yb ratios of Pilbara ultramafic samples range from 0.10 to 0.19 ppm and 1.2–1.7, respectively (**Fig. 7b**). The primitive mantle-normalized (Becker et al., 2006) HSE patterns of the Pilbara samples exhibit similar fractionated patterns characterized by strong Ru enrichment over Os–Ir [$(Ru/Ir)_{PM}$ = 2.0–3.5] and Pt depletion over Os-Ir [$(Pt/Ir)_{PM}$ =0.3–0.6], whereas Pd and Re contents are highly variable (**Fig. 8**). One Pilbara sample (AW52514-4A) shows significantly higher Pd abundance (close to the primitive mantle value) than the rest of the samples. The present-day $^{187}Os/^{188}Os$ values range between ~0.1094 and 0.1166. Rhenium contents are high in two samples (0.13 ppb in AL52614 and 0.35 ppb in AW52514), resulting in superchondritic $^{187}Re/^{188}Os$ (0.53 and 0.86, respectively) and together with consequently unrealistic low initial $^{187}Os/^{188}Os$ values (<0.078) calculated at ~3.4 Ga.

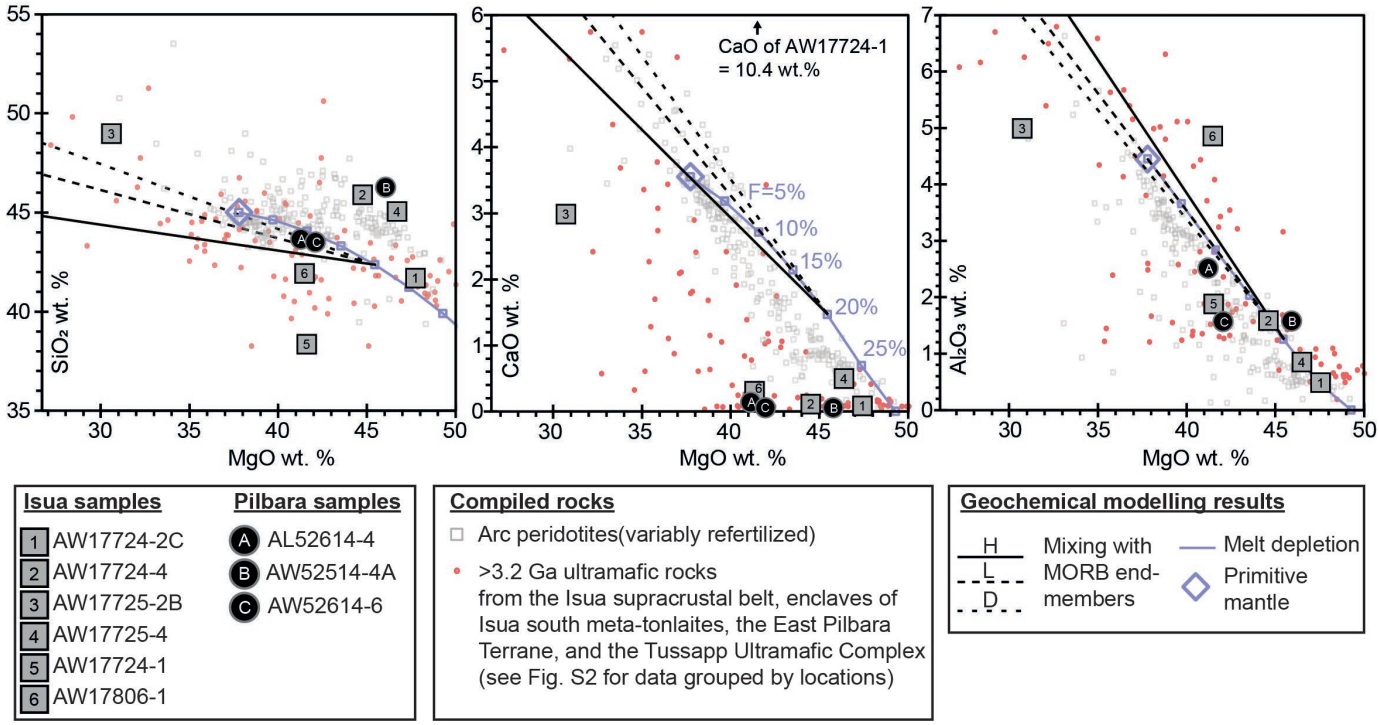

Figure 5. Major element abundances versus Mg# of Pilbara and Isua ultramafic samples. Geochemistry of arc peridotites, other compiled >3.2 Ga ultramafic rocks from the Isua and Pilbara areas, and MELTS modelling results are also plotted for comparison. References of compiled >3.2-Ga ultramafic rocks are listed in the **Fig. 1** caption. All data are presented using anhydrous values (i.e., all major element abundances are normalized to zero LOI and 100 wt.% total). Data for arc peridotites are from Chin et al. (2014) and references therein. Primitive mantle values are from McDonough and Sun (1995). The mixing lines represent mixing between 20% depleted primitive mantle and mid-ocean ridge basalt (MORB) end-members H, L, and D (Elthon, 1992). Details of MELTS modelling are in Chin et al. (2014). Data sources: Serpentinites from the Nob Well Intrusion of the East Pilbara Terrane: Geological Survey of Western Australia 2013 database. Compiled ultramafic rocks from the Isua supracrustal belt: Friend and Nutman (2011), Szilas et al. (2015) and Waterton et al. (2022). Compiled ultramafic rocks from enclaves in meta-tonalite south of the Isua supracrustal belt: Friend et al. (2002); Van de Löcht et al. (2020). Ultramafic rocks from the Tussapp Ultramafic Complex: McIntyre et al. (2019).

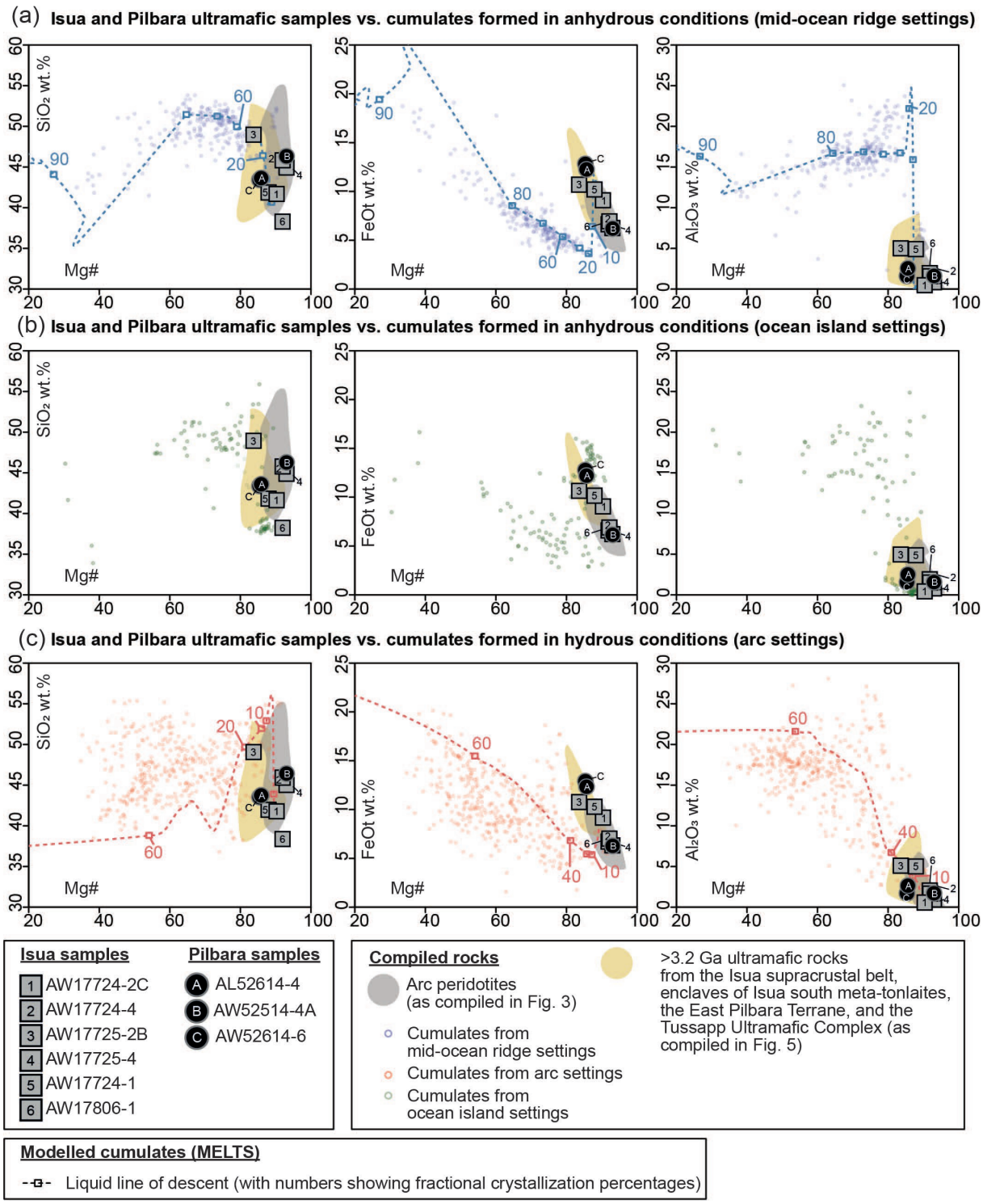

Figure 6. Major element geochemical characteristics of the Isua and Pilbara ultramafic samples in comparison with those of Phanerozoic cumulates, arc peridotites, >3.2 Ga ultramafic rocks (see **Fig. 3** for data sources), and modelled liquid lines of descent. All data are presented using anhydrous values (i.e., all major element abundances are normalized to zero LOI and 100 wt.% total). The data in this figure show that Isua and Pilbara ultramafic rocks, Mg-rich cumulates and mantle peridotites have similar major element geochemical systematics. Data

549 sources for the cumulates and MELTS modelling curves are from Chin et al.
550 (2018), Mallik et al. (2020), and references therein. Specifically, cumulates from
551 oceanic island settings (panel b) cannot be modelled due to limitations of MELTs
552 programs on modelling ultrahigh pressure (>3 GPa) melting and enriched mantle
553 sources, which are necessary for generating oceanic island basalts.

554

555 *4.3.Mineral geochemistry*

556 Olivine grains in Isua sample AW17724-2C (lens B) have extraordinarily high Mg# values
557 of ~95–98 and NiO of ~0.39–0.63 wt.%. In contrast, olivine grains in Isua sample AW17725-
558 4 (lens A) have Mg# values of ~87 and NiO of ~0.52–0.61 wt% (**Table S2**). Ti-humite
559 phases in sample AW17724-2C have variable TiO_2 abundances of ~3.0–8.1 wt.%. All
560 analyzed spinel grains in the Isua samples contain a high magnetite component (i.e., FeOt of
561 ~90 wt.%) (**Table S2**).

562 Spinel of both chromite or magnetite compositions occur in the Pilbara samples.
563 Specifically, chromite spinel grains have Cr_2O_3 of ~40–50 wt.%, TiO_2 of 0.6–4.3 wt.%, and
564 MgO of 5–12 wt.%. The Cr# [Cr/(Cr+Al)] values and Mg# values of chromite spinel grains
565 are ~65–75 and ~17–46, respectively (**Fig. 9**; **Table S2**).

566

567 **5. Discussion**

568 We analyzed phaneritic ultramafic rocks in the Eoarchean Isua supracrustal belt and the
569 East Pilbara Terrane to explore their petrogenesis as a means of testing the viability of
570 existing tectonic models. Specifically, we explore whether these rocks need to be explained
571 as mantle peridotites that were emplaced in the crust in a subduction setting. Our new
572 petrological and geochemical data from six ultramafic samples from the Isua supracrustal belt
573 and three ultramafic samples from the East Pilbara Terrane show that (1) Isua and Pilbara
574 samples have been variably altered and now contain several alteration minerals (e.g.,
575 serpentine and carbonate) that replaced igneous ferromagnesian silicates (**Figs. 2–3**) ; (2)
576 Pilbara ultramafic samples preserve poikilitic textures and polygonal textures (**Fig. 3**); one
577 Isua sample (AW17725-4 from lens A) also preserves relict polygonal textures (**Fig. 2b**); (3)
578 trace element abundances in both Isua and Pilbara ultramafic samples range from depleted
579 with respect to the primitive mantle values (0.1 times primitive mantle values) to enriched
580 (10 times primitive mantle values) (**Fig. 6a–b**); (4) two out of three Pilbara ultramafic
581 samples show fractionated, relatively high concentrations of Os and Ir versus Pt, Pd, and Re

582 in the primitive mantle-normalized diagram (**Fig. 7c**), which are similar to those of Isua meta-
583 peridotite lens samples (Waterton et al., 2022); and (5) chromite spinel in Pilbara ultramafic
584 samples feature Cr# of ~65–75, and Mg# of ~17–46 (**Fig. 9**). In the following sections, we
585 first discuss the potential impacts of alterations on petrology and geochemistry. Then, we
586 show that new and compiled petrology, geochemistry, and microstructures of Isua and Pilbara
587 ultramafic rocks are consistent with a cumulate origin, whereas an origin as thrust-emplaced
588 mantle slices is not consistent with observed geochemistry. We then discuss the implications
589 for testing early Earth tectonic models and the initiation of plate tectonics.

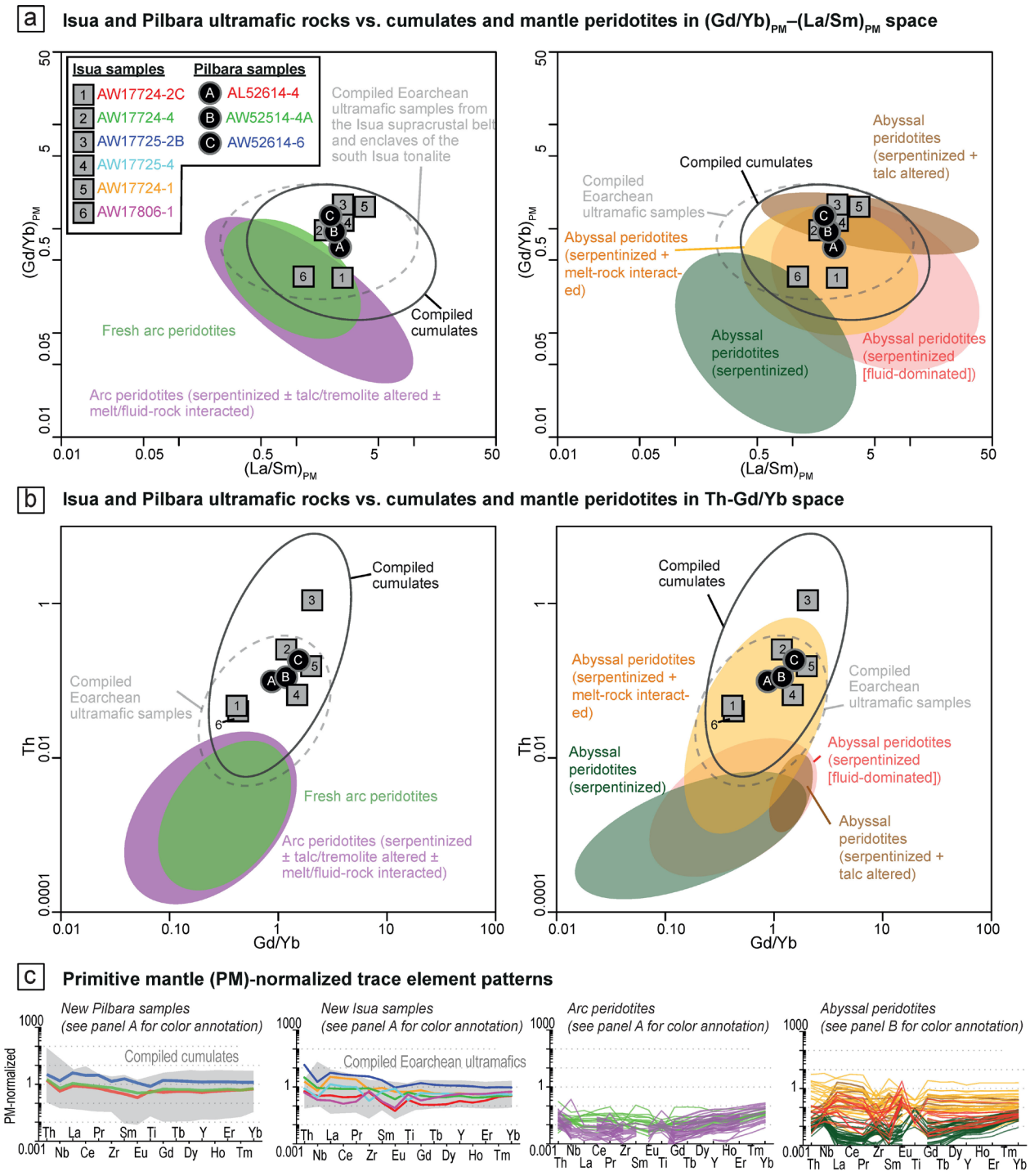

Figure 7. Trace element characteristics for Isua and Pilbara ultramafic samples in comparison with compiled cumulates and variably altered mantle peridotites. **a**, Primitive mantle normalized Gd/Yb and La/Sm ratios [i.e., $(Gd/Yb)_{PM}$ and $(La/Sm)_{PM}$] of investigated samples and compiled rocks. **b**, Th and Gd/Yb ratios of investigated samples and compiled rocks. **c**, Primitive mantle-normalized spider diagrams showing trace element patterns of investigated samples and compiled rocks (see **Figure S4** for spider diagrams grouped by sample locations).

These diagrams show that new and compiled data for ultramafic rocks from the Isua supracrustal belt have similar trace element characteristics to meta-peridotite enclaves from the south Isua meta-tonalites, Pilbara ultramafic samples and other Eoarchean ultramafic cumulates. Only some abyssal peridotites which experienced serpentinization and melt-rock interactions have comparable trace element patterns. Other mantle peridotites have lower Th, Gd/Yb, $(Gd/Yb)_{PM}$, and/or $(La/Sm)_{PM}$ values. Data sources: compiled cumulates involve samples from the Permian Lubei intrusion of NW China (Chen et al., 2018), the late Proterozoic Ntaka Ultramafic Complex of Tanzania (Barnes et al., 2016), the Mesoarchean Nuasahi Massif of India (Khatun et al., 2014), the Mesoarchean Tartoq Group of southwestern Greenland (Szilas et al., 2014), the Mesoarchean Seqi Ultramafic Complex of southwestern Greenland (Szilas et al., 2018), and the Eoarchean Tussapp Ultramafic Complex of southwestern Greenland (McIntyre et al., 2019); compiled Eoarchean ultramafic samples are rocks from the Isua supracrustal belt (Szilas et al., 2015) and the enclaves in meta-tonalite south of the Isua supracrustal belt (Van de Löcht et al., 2020); fresh arc peridotites are from the Kamchatka arc (Ionov, 2010); arc peridotites that experienced serpentnization, talc/tremolite alteration, and/or melt-rock interactions are from the Loma Caribe peridotite body of Dominican Republic (Marchesi et al., 2016) and the Izu-Bonin-Mariana forearc (Parkinson and Pearce, 1998); abyssal peridotites that experienced serpentinization are from the Oman ophiolite (Hanghøj et al., 2010); variably altered abyssal peridotites from the Mid-Atlantic Ridge are summarized by Paulick et al. (2006). Primitive mantle values are from McDonough and Sun (1995).

5.1. Assessment of alteration impacts

Petrological and geochemical information obtained from Isua and Pilbara ultramafic rocks represents the combined effects of petrogenetic processes and alterations. Below we discuss potential types and impacts of alteration on the petrology and geochemistry of these rocks.

High-grade (e.g., granulite facies) metamorphism can lead to partial melting. Partial melting process and subsequent melt-rock interactions can strongly disturb the geochemistry and mineral assemblages of affected rocks. However, the Isua supracrustal belt and the supracrustal rocks in the East Pilbara Terrane (**Fig. 1**) have only experienced amphibolite facies metamorphism (or lower conditions) (e.g., Hickman, 2021; Ramírez-Salazar et al., 2021; Müller et al., in prep.). Both Isua and Pilbara samples show evidence of hydrothermal alterations, as indicated by the dominance of serpentine minerals (**Figs. 2–3**). Therefore, modifications of whole-rock geochemical budgets need to be taken into account (see below). In addition, at mineral scale, chemical changes during metamorphism are possible. For

example, Cr-spinel could be altered to magnetite during metamorphism (e.g., Barnes and Roeder, 2001). Therefore, care must be also taken when interpreting petrogenesis using spinel data.

Fluid assisted alterations could result in changes in mineral assemblages and whole-rock/mineral element concentrations including REEs, but the impacts on fluid-mobile elements (e.g., K, Ca, Si, Rb, Ba and Sr, etc) would be most significant (e.g., Deschamps et al., 2013; Malvoisin et al., 2015; Paulick et al., 2006). Moderate to high LOI contents (~5–21 wt.%; **Fig. 4a**) and the presence of serpentine, talc, and/or magnesite (**Figs. 2–3**) in Isua and Pilbara ultramafic samples show that these rocks have experienced variable degrees of serpentinization, carbonitization, and/or talc-alteration. A ternary plot of anhydrous SiO_2, LOI, and other major element oxides (e.g., MgO, Al_2O_3, **Fig. 4a**) shows that serpentinization is the dominant controlling factor of major element geochemistry as these samples plot near the serpentine mineral composition. Nonetheless, the potential MgO and SiO_2 loss/gain due to serpentinization may be smaller than 5 wt.% for all Isua and Pilbara samples except for two Isua samples AW17725-2B and AW17806-1 (**Fig. 4b**). These two samples show strongly disturbed MgO and SiO_2 as well as significantly enriched Al_2O_3, which cannot be accounted by serpentinization but may be related to melt-rock interactions (see below). Effects of other alterations on major element concentrations and LOI (e.g., Deschamps et al., 2013; Paulick et al., 2006) in most samples appear to be secondary with the exception of sample AW17724-1, which has a high anhydrous CaO concentration (10.4 wt.%). Elevation of CaO in Isua ultramafic rocks has been interpreted as recording calcite addition during carbonitization (Waterton et al. 2022). Although some trace elements like LREEs and Th can be affected by fluid assisted alterations, it is hard to evaluate such effects for Isua and Pilbara samples because trace element systematics can also be strongly affected by primary melt origin and evolution processes such as partial melting, melt fractionation etc. (see below and **Fig. 7**; e.g., Paulick et al. 2006). Some HSEs like Os, Ir, Ru and Pt are relatively immobile during fluid assisted alterations, but Pd and Re could be relatively mobile (e.g., Barnes and Liu, 2011; Büchl et al., 2002; Deschamps et al., 2013; Gannoun et al. 2016). Spinel Al and Cr concentrations can be increased or reduced during fluid-rock interaction, respectively (e.g., El Dien et al., 2019).

Melt-rock interaction is commonly observed in mantle rocks (e.g., Ackerman et al., 2009; Büchl et al., 2002; Deschamps et al., 2013; Niu, 2004; Paulick et al., 2006) where ascending melts react with wall rocks. This process is similar to reactions between cumulate phases and

671 trapped/evolving melts during crystallization or post-cumulus processes (e.g., Borghini and
672 Rampone, 2007; Goodrich et al., 2001; Wager and Brown, 1967). In general, melt-rock
673 interaction can alter the geochemistry of affected rocks towards those of melts at increasing
674 melt/rock ratios (e.g., Kelemen et al., 1992; Paulick et al., 2006). For peridotites interacting
675 with basalts or more evolved melts, the elevation of elements that are relatively enriched in
676 melts (e.g., Si, Ca, Th, Al, Fe, Ti, REEs, Pt, Pd, and Re) is significant (**Figs. 4–7**; e.g.,
677 Deschamps et al., 2013; Hanghøj et al., 2010). Other effects include changes in mineral
678 modes and/or mineral geochemistries (e.g., olivine Mg# reduction; spinel Cr-loss and Al-
679 gain) (e.g., El Dien et al., 2019; Niu and Hekinian, 1997).

680 In summary, fluid/melt rock interaction might in part control the observed geochemistry
681 and petrology of studied Isua and Pilbara samples. Thus, for petrogenetic interpretation, we
682 compare the observed geochemistry and petrology of Isua and Pilbara ultramafic samples
683 with those of cumulates and mantle peridotites that potentially experienced similar alterations
684 (including serpentinization, carbonitization, talc/tremolite alteration, and melt-rock
685 interaction).

686 *5.2. Isua and Pilbara ultramafic rocks are broadly similar*

687 Ultramafic rocks from the East Pilbara Terrane are generally interpreted as cumulates or
688 high-Mg volcanic flows, which are consistent with the widely-accepted non-plate tectonic
689 origin for this terrane (Collins et al., 1998; Hickman, 2021). Therefore, a comparison between
690 Isua and Pilbara ultramafic rocks in terms of their mineralogy, rock textures and whole-
691 rock/spinel geochemistry can be used to explore whether or not they have similar igneous
692 origins, thereby testing the viability of non-plate tectonic models for the Isua supracrustal
693 belt.

694 Isua and Pilbara ultramafic rocks have similar protolith mineralogy and relict olivine
695 polygonal textures, but record different deformation patterns. Serpentine grains preserved in
696 Pilbara samples (**Fig. 3**) appear to be undeformed pseudomorphs after primary olivine and
697 pyroxene. Spinel is abundant in our Pilbara ultramafic samples (**Fig. 3**). Olivine grains
698 preserved in the Isua lens A sample AW17725-4 have forsterite contents of ~87, slightly
699 lower than published forsterite contents of ~88–92 for lens A meta-dunite samples (e.g.,
700 Szilas et al., 2015; Nutman et al., 2020). Olivine grains from lens A samples have been
701 interpreted as primary igneous olivine (e.g., Szilas et al., 2015; Nutman et al., 2020). Other
702 primary minerals observed in Isua ultramafic samples are pyroxene and spinel (**Fig. 2**; e.g.,

Szilas et al., 2015; Nutman et al., 2020; Van de Löcht et al., 2020). Therefore, Isua ultramafic samples potentially have similar protolith mineral assemblages (olivine + spinel ± pyroxene) to their Pilbara counterparts. Pyroxene appears to be a minor component in Pilbara ultramafic samples, and spinifex textures are not observed (**Fig. 3**), which do not support an extrusive komatiite origin for our Pilbara ultramafic samples. Instead, the poikilitic textures of Pilbara ultramafic rocks (**Fig. 3c**) as preserved by the serpentine pseudomorphs can only be explained through the formation of olivine-rich cumulates (Wager and Brown, 1967). The polygonal textures of Pilbara ultramafic rocks (**Fig. 3b**) likely developed via re-equilibration and recrystallization of cumulate olivine grains under crustal conditions (e.g., Hunter, 1996). Therefore, rock textures support the hypothesis that Pilbara ultramafic samples are cumulates. However, primary rock textures of most of our Isua ultramafic samples are lost due to alteration and/or deformation that post-dates olivine and late-stage serpentine minerals (**Fig. 2**). Only one sample (AW17725-4) from the meta-peridotite lens A preserves relict polygonal textures that feature abundant ~120° triple junctions of olivine grains (**Fig. 2b**), consistent with findings in rocks sampled from nearby outcrops (e.g., Nutman et al., 1996) and Pilbara ultramafic samples (**Fig. 3b**). Therefore, relict polygonal textures in Isua lens A samples could also result from mineral re-equilibration and recrystallization under crustal conditions (Hunter et al. 1996) rather than under mantle conditions (Nutman et al., 1996).

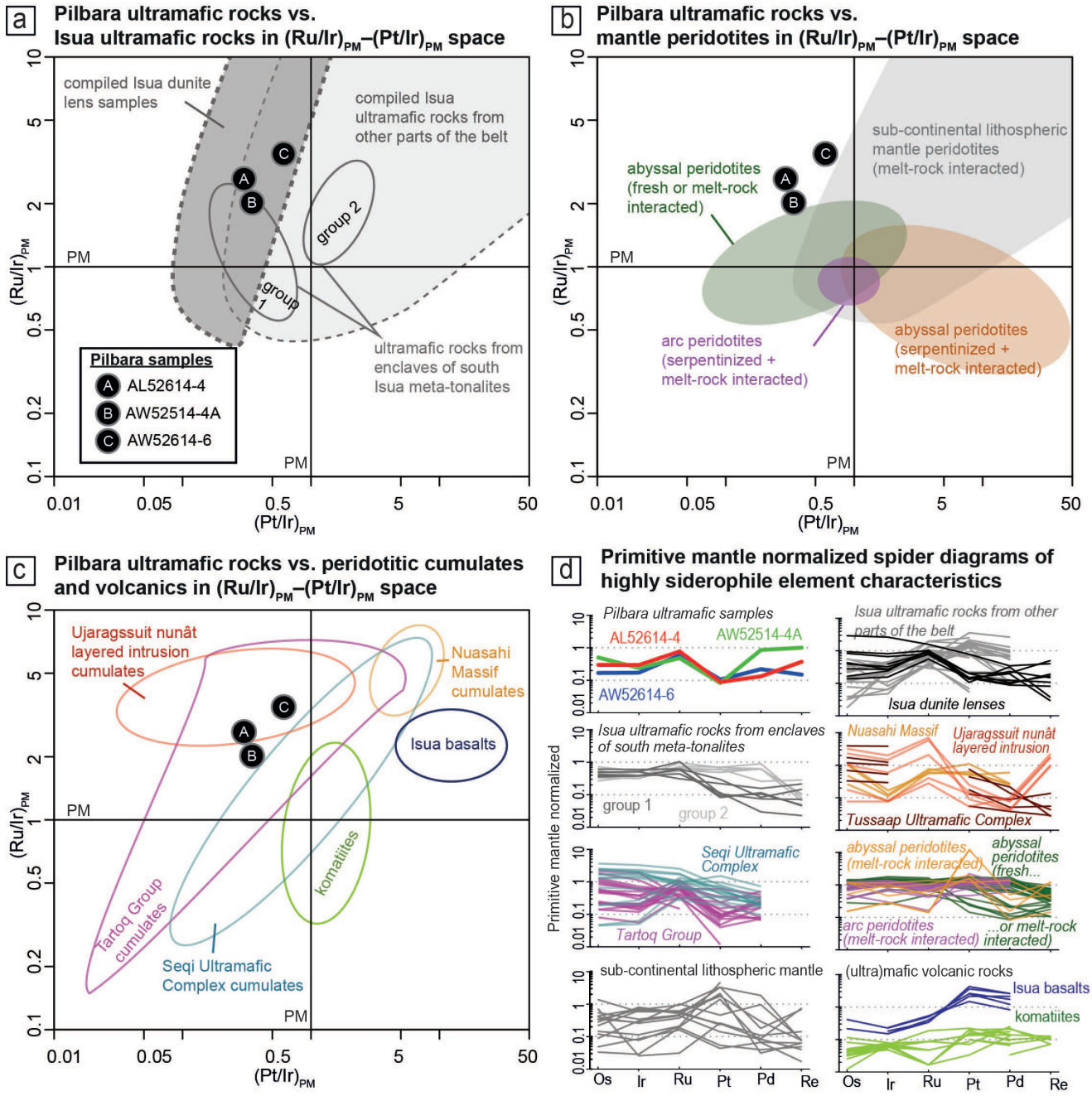

Figure 8. Highly siderophile element (HSE) (including platinum-group elements, PGEs: Os, Ir, Ru, Pt, and Pd) characteristics of the Pilbara samples, Isua ultramafic rocks, cumulates, volcanics and mantle peridotites. Panels **a** to **c** show primitive mantle (PM)-normalized Pt/Ir and Ru/Ir ratios [i.e., $(Pt/Ir)_{PM}$ and $(Ru/Ir)_{PM}$] of new Pilbara samples in comparison with those of Isua ultramafic rocks (from the supracrustal belt and peridotite enclaves, see Figure 4 caption; panel a), mantle peridotites (panel b), volcanics (komatiites and basalts) and peridotitic cumulates (panel c). Peridotites from meta-tonalite enclaves south of

731 the Isua supracrustal belt are divided by Van de Löcht et al. (2018) into two
732 groups according to their HSE signatures: “group 2” peridotites have higher Pt,
733 Pd and Re versus “group 1” peridotites. Panel **d** shows primitive mantle-
734 normalized HSE patterns of new Pilbara samples and compiled rocks in spider
735 diagrams. These plots show that HSE characteristics of Pilbara ultramafic rocks
736 are similar to those of cumulate rocks, but are different from those of mantle
737 peridotites. Furthermore, HSE patterns of ultramafic rocks from peridotite
738 enclaves of meta-tonalites south of the Isua supracrustal belt are consistent with
739 those of cumulates and do not require mantle peridotite origins (cf. Van de Löcht
740 et al., 2018). Data sources: compiled cumulates involve samples from the
741 Eoarchean Ujaragssuit nunât layered intrusion of southwestern Greenland
742 (Coggon et al., 2015) the Mesoarchean Nuasahi Massif of India (Khatun et al.,
743 2014), the Mesoarchean Tartoq Group of southwestern Greenland (Szilas et al.,
744 2014), the Mesoarchean Seqi Ultramafic Complex of southwestern Greenland
745 (Szilas et al., 2018), and the Eoarchean Tussapp Ultramafic Complex of
746 southwestern Greenland (McIntyre et al., 2019); compiled Isua ultramafic
747 samples and basalts are from the Isua supracrustal belt (Szilas et al., 2015) or the
748 peridotite enclaves in meta-tonalite south of the Isua supracrustal belt (Van de
749 Löcht et al., 2018); komatiites are from the Paleoarchean Barberton Greenstone
750 Belt of South Africa (Maier et al., 2003); arc peridotites experienced
751 serpentinization and melt-rock interaction are from the Northwest Anatolian
752 orogenic complex, Turkey (Aldanmaz and Koprubasi, 2006); fresh and variably
753 melt-refertilized abyssal peridotites are from the collisional massifs in Italian
754 Alps, Italy (Wang et al., 2013); abyssal peridotites that experienced
755 serpentnization and melt-rock interaction are from the Troodos Ophiolite
756 Complex of Cyprus (Büchl et al., 2002); sub-continental lithospheric mantle
757 rocks that experienced melt-rock interactions are from the Bohemian Massif of
758 the Czech Republic (Ackerman et al., 2009). Primitive mantle values: Becker et
759 al. (2006).

760

761 Ultramafic samples from the Isua supracrustal belt have similar major and trace element
762 geochemistry to the Pilbara ultramafic samples (see below; **Figs. 4–9**). Three Isua ultramafic
763 samples (AW17724-2C, AW17724-4, and AW17725-4) from meta-peridotite lenses show

similar compositions to three Pilbara ultramafic samples in MgO–SiO_2, MgO–CaO, and MgO–Al_2O_3 spaces (**Fig. 5**). Three Isua ultramafic samples collected from the Isua supracrustal belt outside of the lenses either have extraordinarily low MgO (AW17725-2B), high CaO (AW17724-1), or high Al_2O_3 (AW17725-2B and AW17806-1). Both Isua and Pilbara ultramafic samples show similar normalized trace element abundances (i.e., ~0.1–10 times PM). In primitive mantle-normalized diagrams, the Pilbara ultramafic samples show fractionated LREE trends [with $(La/Sm)_{PM}$ of ~1.9–2.4], and generally unfractionated heavy REE [with $(Gd/Yb)_{PM}$ of ~0.8–1.2] (**Fig. 7a**). Such fractionation trends are consistent with some Isua ultramafic samples [note that all Isua samples have $(La/Sm)_{PM}$ of ~1.1–3.8 and $(Gd/Yb)_{PM}$ of ~0.3–1.6; **Fig. 7a**]. The Th concentrations and Gd/Yb ratio also have significant overlaps (Isua versus Pilbara ultramafic rocks: ~0.04–1.13 versus ~0.10–0.19 ppm; ~0.4–2.1 versus 1.2–1.7, respectively; **Fig. 7b**).

Pilbara ultramafic samples appear to have similar HSE patterns compared to the Isua meta-peridotite lens samples [compiled from Waterton et al. (2022); **Fig. 8a**], highlighted by their overlapping $(Pt/Ir)_{PM}$ (~0.3–0.6 Pilbara vs ~0.2–0.9 Isua meta-peridotite lenses) and $(Ru/Ir)_{PM}$ (~2.0–3.5 Pilbara vs ~0.5–10.0 Isua meta-peridotite lenses) ratios. Compiled ultramafic rocks from other parts of the Isua supracrustal belt (Szilas et al., 2015) have much broader ranges of $(Pt/Ir)_{PM}$ (~0.5–26.1) and $(Ru/Ir)_{PM}$ (~0.6–18.2) values, which largely encompass the Pilbara ultramafic rocks but extended to much higher $(Pt/Ir)_{PM}$. "Group 1" peridotites from ultramafic enclaves in the meta-tonalite south of the Isua supracrustal belt (**Fig. 8a**; Van de Löcht et al., 2018) have unfractionated to slightly fractionated Os-Ir-Ru elements [with $(Ru/Ir)_{PM}$ of ~0.6–2.0] and relatively low Pt and Pd versus I-PGE [with $(Pt/Ir)_{PM}$ of ~0.2–0.5], which are similar to some Isua lenses A and B samples featuring lower Ru enrichment than Pilbara ultramafic samples.

Spinel (chromite and magnetite) from the Pilbara ultramafic samples show similar chemistry to those of new and compiled ultramafic samples from the Isua supracrustal belt. Chromite yields relatively constant Cr# (~60–80), but variable Mg# (~20–50), and highly variable TiO_2 (~0.5–5.0 wt.%). Only magnetite was found in our Isua ultramafic samples from the meta-peridotite lenses, which shows low TiO_2 (<0.5 wt.%), high Cr# (>90), and low Mg# (<20) (**Fig. 9**). Compiled ultramafic samples from the meta-peridotite lenses of the Isua supracrustal belt contain both chromite and magnetite (Szilas et al., 2015). Most of the compiled chromite from these samples shows similar Mg# and Cr# values to the chromite

from the Pilbara samples. Other chromite yields Mg# and Cr# trends towards the magnetite composition (**Fig. 9**). The compiled chromite also shows variable TiO_2 (~0.2–2.4 wt.%).

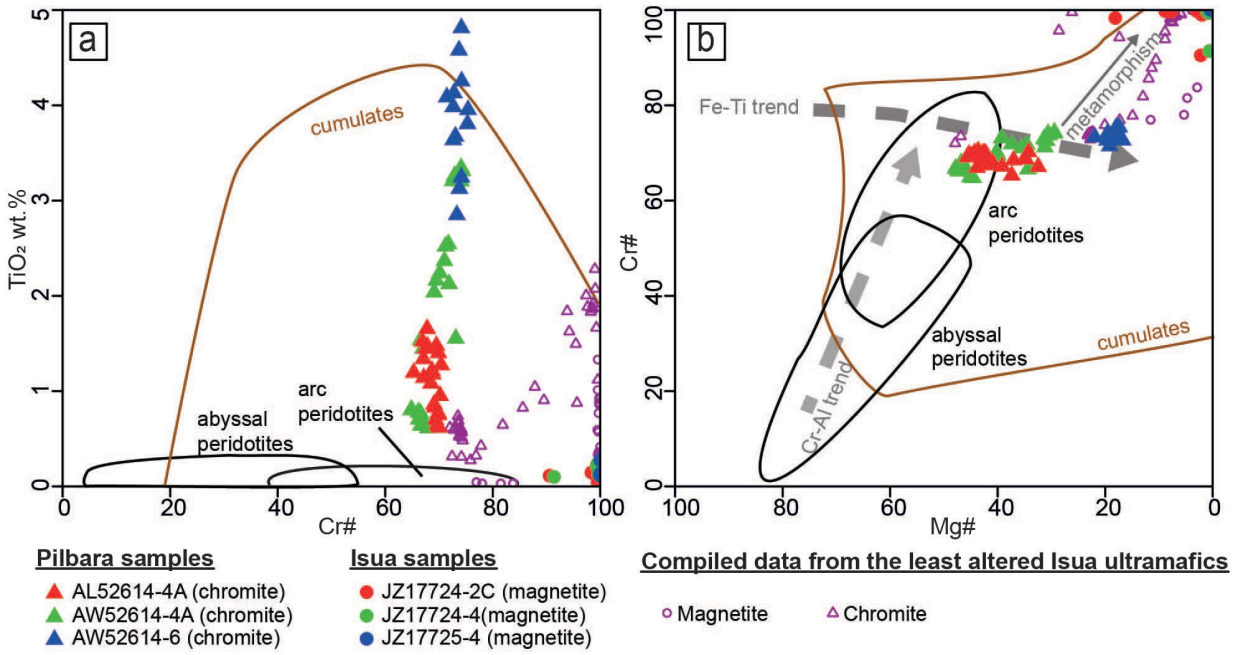

Figure 9. Geochemical signatures of spinel in Pilbara and Isua samples, plotted with compiled fields for ultramafic cumulates and mantle peridotites. Panel **a** shows Cr# values [Cr/(Cr+Al)] and TiO_2 concentrations of spinel. Panel **b** shows Mg# [Mg/(Mg+Fe)] and Cr# values of spinel. The Fe–Ti trend of spinel (representing equilibration during fractional crystallization) and the Cr–Al trend of spinel (representing equilibration in mantle) are plotted for comparison. These plots indicate that spinel from Isua and Pilbara samples are similar to those of cumulates, but are different from those of mantle peridotites. Data sources: compiled spinel from Isua ultramafic rocks: Szilas et al. (2015); the spinel field of cumulates is fit by spinel data from the Uralian-Alaskan type intrusions (Abdallah et al., 2019; Garuti et al., 2003; Himmelberg and Loney, 1995; Krause et al., 2011; Thakurta et al., 2008), the Mesoarchean Seqi Ultramafic Complex of southwestern Greenland (Szilas et al., 2018) and data compiled in Barnes and Roeder (2001); the spinel field of arc peridotites is fit by spinel data in Ionov (2010), Parkinson and Pearce (1998) and Tamura and Arai (2006); the spinel field of abyssal peridotites is fitted by spinel data in Khedr et al. (2014), Standish et al. (2002) and Tamura and Arai (2006). Spinel Fe-Tl, Cr-Al and metamorphic trends are from Barnes and Roeder (2001).

In summary, polygonal textures found in Isua ultramafic rocks (i.e., polygonal textures) also occur in Pilbara ultramafic samples. Pilbara ultramafic rocks potentially have similar primary mineral assemblages (olivine + spinel ± pyroxene) compared to those of the Isua ultramafic rocks, although their alteration and deformational overprints differ. Ultramafic

822 rocks from the Isua supracrustal belt show broadly similar HSE characteristics to those found
823 in the Pilbara ultramafic rocks, although peridotites from enclaves in the meta-tonalite body
824 south of the Isua supracrustal belt exhibit lower $(Pt/Ir)_{PM}$ values. The rocks have broadly
825 similar geochemical characteristics in other whole-rock major and trace elements and spinel
826 geochemistry. On the other hand, with our serpentinized Pilbara sample set, possibly similar
827 olivine microstructures or oxygen isotopic systematics cannot be evaluated in detail.

828 *5.3. REE-HSE signatures of Isua and Pilbara ultramafic rocks are not consistent with*
829 *metasomatised mantle residues*

830 Isua and Pilbara ultramafic rocks show flat or mildly fractionated trace element
831 abundances 0.1 to 10 times primitive mantle values with ~1.1 to ~3.8 $(La/Sm)_{PM}$ and ~0.3 to
832 ~1.7 $(Gd/Yb)_{PM}$ (**Fig. 7**). These patterns cannot be attributed to depleted mantle rocks that
833 exhibit significantly lower Th, LREE and $(Gd/Yb)_{PM}$ due to melt depletion (**Fig. 7a**). Instead,
834 the level of trace element enrichment in Isua and Pilbara ultramafic rocks, especially as
835 shown by Th-Gd/Yb systematics (**Fig. 7b**), can only be explained by melt-rock interactions.
836 Therefore, previous studies interpreted that Isua meta-peridotites from lenses A and B are
837 sub-arc mantle residues interacted with co-existing arc basalt magmas (Friend and Nutman,
838 2011), whereas those from the southern meta-tonalite enclaves are mantle residues interacted
839 with adakitic slab melts (Van de Löcht et al. 2020). Below, we show that these interpretations
840 cannot explain the HSE patterns obtained for these rocks. Instead, the REE-HSE patterns of
841 Isua and Pilbara ultramafic rocks reflect olivine-rich cumulates interacted with co-existing
842 melts from crustal magma chambers or deep, potentially reduced mantle. Therefore, no
843 ultramafic protoliths nor melt components require plate tectonic subduction at Isua.

844 Mantle residues metasomatised by slab melts have radiogenic Os isotopic signatures
845 inherited from recycled crustal materials (Brandon et al., 1996; Gannoun et al.,2016).
846 However, Isua ultramafic rocks collectively exhibit unradiogenic Os isotopic signatures (Van
847 de Löcht et al., 2018; Waterton et al., 2022; this study). Therefore, Isua ultramafic rocks
848 cannot be explained by melt-rock interactions involving slab melts (cf. Van de Löcht et al.
849 2020).

850 To reproduce REE patterns of Isua and Pilbara ultramafic rocks in the context of mantle
851 residue origins, mixing between mantle residues (see Supplementary information for details
852 on modelling) and up to ~20% co-existing basaltic melts would be required (**Fig. 10a**).
853 However, such mixing proportions would significantly impact the HSE concentrations of

metasomatised ultramafic rocks (**Fig. 10a**). This is because basaltic magmas, in comparison to mantle rocks, typically have fractionated HSE patterns characterized by the enrichment of Pt–Pd and Re with respect to IPGE (e.g., Bockrath et al. 2004; Fiorentini et al. 2010; Brenan et al., 2016). For example, the limited HSE data for Isua tholeiitic basalts yield Pt and Pd abundances of ~11 and ~6 ppb, respectively (**Fig. 10a**; Szilas et al. 2015); both values well-above common values typical for mantle peridotites. Thus, plausible mixing with such melts cannot generate low Pt and Pt contents preserved in Isua and Pilbara ultramafic rocks (**Fig. 10a**). By contrast, the observed signatures of the Isua and Pilbara ultramafic rocks predict that interacted melt must contain relatively high REE, but at the same time, low Pt and Pd contents (both compared to primitive mantle).

Sulphide removal during magma crystallization (e.g., Lightfoot and Keays, 2005) is a mechanism that can lower the Pt and Pd abundances of the co-genetic melts. In Isua and Pilbara, some meta-basalt layers were found to contain sulphide minerals which crystallized coevally with the basalts (Appel, 1979; Hickman, 2021). Therefore, at least some Isua and Pilbara basalts may have undergone sulphide exhaustion that would lead to low HSE concentrations in the remaining melt (see **Fig. 10b** for low HSE contents of basalts after sulphide removal; Lightfoot and Keays, 2005; Wooden et al., 1993). Consequently, mixing between ultramafic protoliths and such low HSE basalts can generate observed HSE and REE patterns (**Fig. 10b**). It is important to note, that sulphide removal from basaltic melts is restricted to crustal levels (e.g., Arndt et al., 2005) and therefore, mantle residues cannot interact with such low HSE melts.

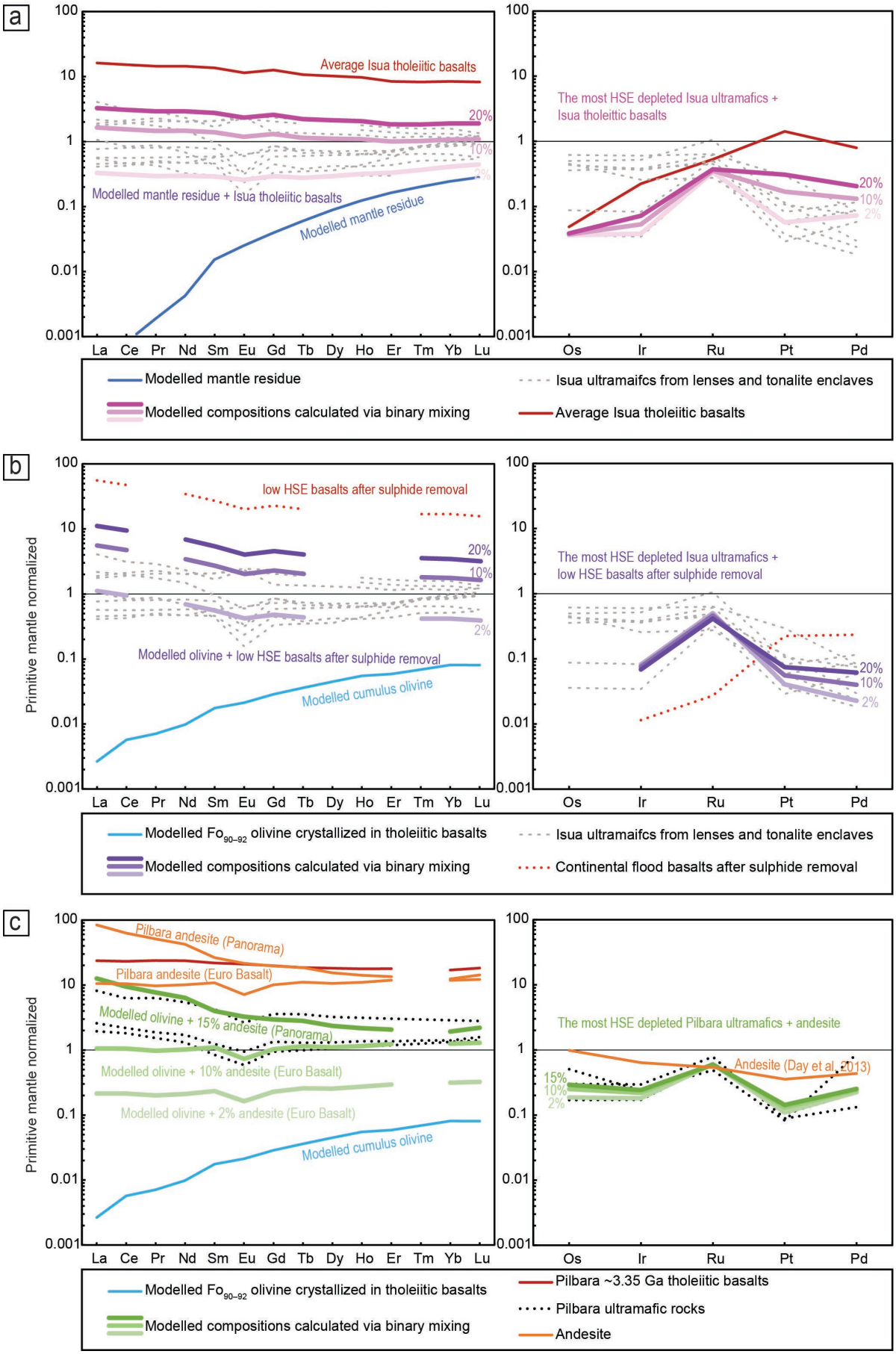
a
Average Isua tholeiitic basalts
20%
10%
2%
Modelled mantle residue + Isua tholeiitic basalts
Modelled mantle residue
The most HSE depleted Isua ultramafics + Isua tholeittic basalts
La Ce Pr Nd Sm Eu Gd Tb Dy Ho Er Tm Yb Lu
Os Ir Ru Pt Pd
Modelled mantle residue
Isua ultramaifcs from lenses and tonalite enclaves
Modelled compositions calculated via binary mixing
Average Isua tholeiitic basalts
b
Primitive mantle normalized
low HSE basalts after sulphide removal
Modelled olivine + low HSE basalts after sulphide removal
Modelled cumulus olivine
The most HSE depleted Isua ultramafics + low HSE basalts after sulphide removal
Modelled Fo90–92 olivine crystallized in tholeiitic basalts
Isua ultramaifcs from lenses and tonalite enclaves
Modelled compositions calculated via binary mixing
Continental flood basalts after sulphide removal
c
Primitive mantle normalized
Pilbara andesite (Panorama)
Pilbara andesite (Euro Basalt)
Modelled olivine + 15% andesite (Panorama)
Modelled olivine + 10% andesite (Euro Basalt)
Modelled olivine + 2% andesite (Euro Basalt)
Modelled cumulus olivine
The most HSE depleted Pilbara ultramafics + andesite
Andesite (Day et al., 2013)
15%
10%
2%
Modelled Fo90–92 olivine crystallized in tholeiitic basalts
Modelled compositions calculated via binary mixing
Pilbara ~3.35 Ga tholeiitic basalts
Pilbara ultramafic rocks
Andesite

876

877 **Figure 10**: Primitive-mantle normalized REE (McDonough and Sun, 1995) and
878 HSE (Becker et al., 2006) patterns of Isua (panels a and b) and Pilbara (panel b)
879 ultramafic rocks, compared to modelled and compiled mineral and/or whole-rock
880 compositions of potential mixing components or their chemical equivalents.
881 Binary mixing models considered here involve one rock component (mantle
882 residue or cumulate) and one melt component (e.g., basaltic melt). The REE
883 compositions of mantle residue are from geochemical modelling (see
884 Supplementary Information). REE compositions of other rock or melt
885 components are compiled from the literature. For HSEs, the most HSE depleted
886 ultramafic sample in Isua or Pilbara with potentially co-genetic melts were
887 subject to mixing to examine the corresponding changes in Pt and Pd contents.
888 Because the HSE data for Pilbara andesites are not available, we adopt the HSE
889 composition of andesite studied by Day et al. (2013). Mixing models show that
890 Isua and Pilbara ultramafic rocks can be best explained by mixing between
891 olivine-cumulates and co-genetic low HSE melts. Such low HSE melts can be
892 formed by deep mantle melting (potentially under reduced conditions), or
893 sulphide removal or fractional crystallization in magma chambers. Data sources:
894 REE values of modelled cumulate olivine are from Waterton et al. (2022);
895 average REE values of Isua tholeiitic basalts are taken from the least altered
896 samples measured by Polat and Hofmann (2003); HSE compositions of Isua
897 tholeiitic basalts are taken from a single sample measured by Szilas et al. (2015);
898 average Pilbara tholeiitic basalts and andesites are from the ~3.35 Ga Euro Basalt
899 Formation and/or the ~3.43 Ga Panorama Formation of the East Pilbara Terrane
900 (Smithies et al. 2007); continental flood basalts after sulphide removal are from
901 Lightfoot and Keays (2005) and Wooden et al. (1993).

902

903 Low HSE melts can be also generated due to retention of HSE-rich phases (sulphide
904 and/or PGE-bearing alloys) in the mantle residues after melting (e.g., Fiorentini et al., 2011;
905 Waterton et al., 2021). While there are several possibilities how to retain sulphide or PGE-
906 bearing alloy as melt residues, none of them appears to be consistent with partial melting in
907 an Eoarchean mantle wedge. First, sulphur is less soluble in melts under higher pressures
908 (O'Neill and Mavrogenes, 2002), while mantle-derived HSE-poor melts indicate deep mantle
909 sources (e.g., low HSE komatiites; Fiorentini et al., 2011). Second, Pd might become

910 compatible in majoritic garnets, and PGE-alloys might be stable in deep mantle (e.g., >7
911 GPa; Waterton et al., 2021 and references therein). Third, PGE-alloys can be stable under
912 reduced mantle conditions even during high degree partial melting (e.g., Fiorentini et al.,
913 2011). Therefore, the potential presence of low Pt and Pd Isua tholeiitic basalts may be
914 explained by deep mantle melting and/or reduced mantle environments, which are
915 inconsistent with a mantle wedge setting that predicts shallow mantle melting as well as
916 relatively oxidized environments (e.g., Figure 8 of Nutman et al., 2013a; Smart et al., 2016).
917 On the other hand, retention of PGE-bearing phases in residues and generation of low HSE
918 basalts (or komatiites) are possible via plume or heat-pipe style mantle melting (Fiorentini et
919 al., 2011; Waterton et al., 2021; Moore and Webb, 2013; Smithies et al., 2007).

920 Mixing with low HSE melts formed by progressive fractional crystallization of parental
921 basaltic magmas is another possible scenario that might explain the HSE-REE composition of
922 Isua and Pilbara ultramafic rocks (**Fig. 10c**). For example, in the East Pilbara Terrane, minor
923 andesites can be found in thick (ultra)mafic to felsic volcanic successions (Smithies et al.
924 2007), which may be co-genetic with lava fractional crystallization. These andesites (SiO_2 ≈
925 54 to 61 wt.%) have flat to mildly fractionated REE patterns (**Fig. 10c**). Binary mixing
926 models show that 10% to 15% mixing between cumulate olivine (Waterton et al. 2022) and a
927 component with Pilbara andesite REE compositions can successfully reproduce REE
928 systematics of Pilbara ultramafic rocks, especially their mildly fractionated LREE and
929 negative Eu anomalies (**Fig. 10b**) which cannot be accounted only by mixing with potentially
930 coeval Pilbara tholeiitic basalts (**Fig. 10b**). Although no HSE data are available for these
931 andesites, limited data obtained so far for melts with similar andesitic composition (Day et al.
932 2013) indicate generally low HSE contents in such a melt type (e.g., Pt and Pd <3.1 ppb).
933 Thus, we envision that REE/HSE abundances of Pilbara ultramafic rocks can be best
934 explained by mixing with Pilbara andesites (**Fig. 10b**). Similarly evolved, but now altered
935 andesitic rocks exist in the Isua supracrustal belt (Nutman et al., 2010). The enriched,
936 fractionated REEs and negative Eu anomalies in some Isua ultramafic rocks indicate mixing
937 with andesitic melts that compositionally similar to Pilbara andesites (**Figs. 7, 10a**). It is
938 again impossible for mantle residues to become mixed with such evolved, low HSE melts
939 generated by fractional crystallization of parental magmas during their ascent at crustal
940 levels.

941 The Nb depletion relative to Th and La, which exists in both Isua ultramafic rocks and
942 Isua basalts (Fig. 7; Polat and Hofmann, 2003), has been ascribed to support melt-rock

943 interactions with volcanic arc basalts. In this Eoarchean plate tectonic scenario, Nb (and Ta)
944 depletion would indicate effects of either fluids or melting in the presence of rutile associated
945 with progressive dehydratation and/or melting of a downgoing subducted slab (e.g., Münker,
946 1998; Keppler, 1996). However, it needs to be pointed out that this signature is not unique to
947 volcanic arcs, particularly with respect to the early Earth. For example, basalts, felsic
948 volcanics, TTGs, and ultramafic rocks (**Fig. 7c**) of the East Pilbara Terrane collectively also
949 exhibit strong Nb depletion (e.g., Martin et al. 2005; Smithies et al. 2007), while this terrane
950 has been attributed to be plume-generated in a stagnant-lid tectonic setting (e.g., Van
951 Kranendonk et al. 2007). Furthermore, rutile as well as fluids can also form during
952 metamorphic dehydration of the lower parts of the thickened lithosphere in non-plate tectonic
953 settings (Johnson et al., 2017), particularly in a heat-pipe lithosphere featuring cold geotherm
954 (Moore and Webb, 2013). Recycling of such lower crust materials (which is possible in plate
955 and non-plate tectonic settings via mechanisms like delamination, sagduction and/or
956 downwards advection) and subsequent fluid flux and melting could generate igneous rocks
957 with Nb-Ta depletion. Alternatively, Nb depletion may be a secondary signature formed via
958 fluid metasomatism under amphibolite facies conditions (Guice et al., 2018). Vigorous fluid
959 activities and material exchanges between mantle and crust in non-plate tectonic settings can
960 also explain the mantle-like $\delta^{18}O$ signatures found in some Isua olivines (Nutman et al.
961 2021a). Indeed, mantle-like oxygen isotope values are observed in zircons from some TTGs
962 (originally lower crust partial melts) of the East Pilbara Terrane (Smithies et al., 2021). This
963 finding implies a fluid-rich early mantle, buffered by fluxing from the recycled crust, that was
964 capable of introducing mantle-like oxygen isotope signatures to early crust and associated
965 magmas (Smithies et al., 2021).

966 To conclude, to explain the observed REE-HSE characteristics of Isua and Pilbara
967 ultramafic rocks, mixing with REE-enriched, but HSE-depleted (relative to primitive mantle)
968 melt is required. Possible candidates are (1) tholeiitic basalt or komatiite derived from deep,
969 potentially reduced mantle (likely associated with plume or heat-pipe melting); (2) melts that
970 have undergone sulphide removal (limited to crustal levels); and (3) evolved melts formed
971 through fractional crystallization of ascending parental basaltic magmas. With the exception
972 of the first candidate, mantle residues cannot interact with these melts. The first candidate
973 cannot interact with sub-arc depleted mantle. Alternatively, mixing cumulus olivine ±
974 chromite ± orthopyroxene with those REE-enriched, but HSE-depleted melts can explain the
975 formation of both Isua and Pilbara ultramafic rocks (**Figs. 7–8, 10**), along with potentially

other Eoarchean ultramafic cumulates which show similar REE and HSE geochemistry (Coggon et al. 2015; McIntyre et al. 2019).

5.4. Do any features preserved in Isua and Pilbara ultramafic rocks require formation in mantle?

Comparison between our findings and those of similarly altered compiled and modelled cumulates and mantle peridotites show that no geochemical, petrological, and textural characteristics preserved in Isua and Pilbara ultramafic rocks require formation in mantle.

Pilbara ultramafic rocks, which preserve cumulate textures (**Fig. 3**), have similar whole-rock major and trace element geochemistry as many mantle peridotites (**Fig. 5-8**). However, other compiled and modelled whole-rock data also show that olivine-rich cumulates could be geochemically similar to variably depleted and subsequently melt-metasomatised mantle rocks in terms of many whole-rock major element systematics (e.g., MgO, SiO_2, Al_2O_3, FeOt, trace elements; **Figs. 5-8, 11**). In addition, olivine-rich cumulates and mantle residue may have similar protolith mineralogy of olivine ± pyroxene ± spinel. Although clinopyroxene inclusions in olivine have been interpreted as reflecting melt-rock interactions in mantle (Nutman et al., 2021a), we argue that clinopyroxene undersaturation and olivine saturation are possible across a range of pressure-temperature-composition combinations (Chen and Zhang, 2009 and references therein) and could happen under crustal conditions during magma crystallization in the presence of water, crustal assimilation and/or magma recharge (e.g., Kelemen, 1990; Gordeychik et al., 2018).

Geochemistry of primary chromite grains of both Isua and Pilbara ultramafic samples indicates equilibrium during magma crystallization rather than equilibrium with mantle olivine. New and compiled and Pilbara chromite grains match the Fe–Ti trend in the Mg#–Cr# space (**Fig. 9b**). Such a trend can be produced by equilibration of spinel phases during fractional crystallization (Barnes and Roeder, 2001), and thus can be found in cumulates (**Fig. 9b**). Chromite crystals of Isua and Pilbara samples also have variable TiO_2 (up to ~2 and ~5 wt.%, respectively). In contrast, due to equilibration with olivine, mantle spinel typically has high Mg# and varied Cr# (i.e., the Cr–Al trend in **Fig. 9b**, Barnes and Roeder, 2001) as well as low TiO_2 (typically <1 wt.%; **Fig. 9a**) (e.g., Tamura and Arai, 2006). Although fluid/melt assisted alterations could impact chromite geochemistry in mantle rocks, expected changes include Cr# reduction and Mg# increase along with the Cr–Al trend (El Dien et al., 2019), which are not consistent with the observed spinel geochemistry.

Although the B-type olivine fabrics (Kaczmarek et al., 2016) have been interpreted to reflect mantle environments, they are also consistent with cumulate origins because such fabrics can form via magmatic or metamorphic processes (e.g., Chin et al., 2020; Holtzman et al., 2003; Nagaya et al., 2014; Yao et al., 2019) rather than via deformation in mantle wedge (cf. Kaczmarek et al. 2016). The relationships between olivine crystal axes and sample lineation support metamorphic origins of B-type fabrics for Isua lens B samples: olivine preserved there is considered to be dehydration products of antigorite-breakdown (e.g., Guotana et al. 2022). Alignment of olivine shape long-axes in lens B (see Fig. 1D of Nutman et al. 2021a) generally parallel to the regional lineation directions (mostly trending southeast; Zuo et al. 2021). If olivine long-axes correspond to their [001] crystal directions as suggested by Kaczmerak et al. (2016), then olivine [001] is generally parallel with lineation directions, which are also antigorite (010) directions in deformed serpentinites (e.g., Nagaya et al. 2017). Such crystal axis relationships are consistent with a metamorphic origin of olivine B-type fabrics, in which topotactic growth of olivine occurred with olivine [001] axes parallel to antigorite (010) (Nagaya et al. 2014). Therefore, with current rock and mineral textural data from Isua ultramafic rocks, mantle wedge conditions are not required, and cumulate origins are viable.

Finally, the presence of Ti-humite in Isua ultramafic rocks has been interpreted to reflect low-temperature, UHP (i.e., <500 °C, >2.6 GPa) metamorphism (Friend and Nutman, 2011; Nutman et al., 2020; Guotana et al., 2022) primarily using the petrogenetic grid generated from experiments (i.e., Shen et al. 2015). However, our complementary work (Müller et al., in prep.) shows that the results of Shen et al. (2015) cannot be directly applied to Isua ultramafic rocks. This is because Shen et al. (2015) experimented on a CO_2-free chemical system, but Isua ultramafic rocks preserve carbonate phases (**Fig. 2a**) that appear to be a reaction product of an olivine-breakdown reaction, equally producing antigorite and Ti-humite (Müller et al., in prep.). Conversely, Müller et al. (in prep.) show that Ti-humite could have been formed under much lower pressures, such as the amphibolite facies conditions recorded by the other parts of the belt (Ramírez-Salazar et al., 2021). Therefore, the Isua supracrustal belt may not have experienced (U)HP metamorphism, obviating the need for plate tectonic subduction (Waterton et al., 2022; cf. Friend and Nutman, 2011; Nutman et al., 2020; Guotana et al., 2022).

5.5. A model for emplacement, metamorphism and alteration of Eo- and Paleo-Archean phaneritic ultramafic rocks

Our analyses show that the Isua and Pilbara ultramafic rocks preserve no igneous and alteration signature that requires to be interpreted by tectonically-emplaced metasomatised mantle residue. Rather, the rock textures of Pilbara samples and the REE-HSE characteristics of both Isua and Pilbara samples require them to be olivine-rich cumulates that interacted with low HSE melts of non-arc origins. Our findings reject the hypothesis that some Isua ultramafic rocks represent unique examples of earth's earliest tectonically-exhumed mantle, which indicate the Eoarchean operation of plate tectonics (cf. Nutman et al., 2020, 2021a; Van de Löcht et al., 2018, 2020), but suggest these Isua ultramafic rocks are similar with other Eo- and Paleoarchean phaneritic ultramafic rocks – originally crystallized as crustal cumulates.

Here we describe a common evolutionary pathway for ultramafic rocks of early Earth terranes in the context of the hot stagnant-lid tectonic regimes such as heat-pipe tectonics (Moore and Webb, 2013) and partial convective overturn tectonics (Collins et al., 1998), which have been proposed for such terranes. Ultramafic rocks of early Earth could have initially crystallized from high-magnesium, fluid-rich magmas, either as ultramafic volcanic flows [e.g., komatiites, Byerly et al. (2019)], intrusions, or crustal cumulates at the bases of lava flows or magma chambers (**Fig. 11**). Some of these rocks could have experienced interactions with co-genetic, low HSE melts from deep mantle or magma chamber (**Fig. 11**). Later, these ultramafic rocks could have been metamorphosed under crustal conditions (e.g., greenschist or amphibolite facies conditions) that may or may not have been associated with significant deformation and mineral phase transformation. In the case of the Isua supracrustal belt, amphibolite facies metamorphism was accompanied by deformation during, at the end of, or after heat-pipe cooling (e.g., Ramírez-Salazar et al., 2021; Webb et al., 2020; Zuo et al., 2021). These P-T conditions are capable of producing serpentine ± Ti-humite ± carbonate via olivine breakdown reactions (**Fig. 11a**; Müller et al., in prep). Primary igneous textures in olivine-rich cumulates could have been preserved by concentrating most of the strain into other phases (e.g., Yao et al., 2019; Zuo et al., 2021). Alternatively, growth of metamorphic olivine from dehydration breakdown of strongly oriented serpentine minerals could also produce a B-type olivine CPO (e.g., Nagaya et al., 2014). In contrast, hot stagnant-lid volcanism during the Paleoarchean time would have been less rapid in terms of long-term deposition and burial rates versus the Eoarchean Isua supracrustal belt, and thus would have led to a relatively hot lithosphere for the East Pilbara Terrane (Moore and Webb, 2013; Webb et al., 2020), potentially permitting intra-crustal partial convection via gravitational instability

(**Fig. 11b**; Collins et al., 1998). The metamorphic conditions experienced by the exposed Pilbara rocks may have been lower, and deformation may have been weaker (e.g., Collins et al., 1998; Wiemer et al., 2018), especially in rocks located far from the margins of the granitoid bodies (e.g., François et al., 2014) such as the samples studied here (**Fig. 1b**). Consequently, Pilbara ultramafic samples only preserve evidence for greenschist facies metamorphism without identifiable strain (**Fig. 3**). Post-deformational alterations (such as carbonate or serpentine alterations) might have further modified these ultramafic rocks as well as nearby supracrustal rocks in the following >3 billion years (**Fig. 11**).

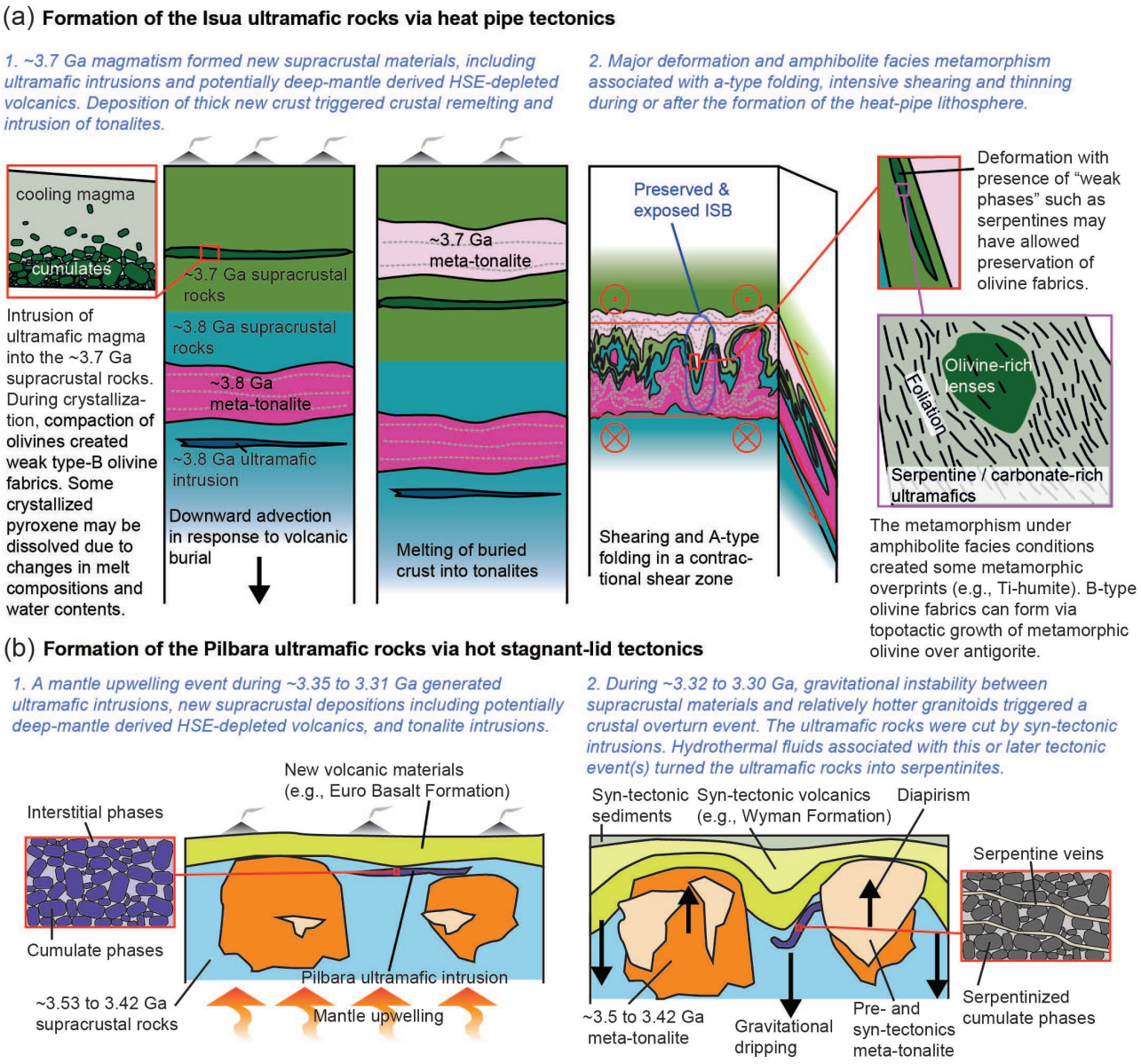

Figure 11. Evolutionary diagrams for Isua and Pilbara ultramafic rocks. Ultramafic rocks from both terranes can be interpreted via similar hot stagnant-lid tectonic models. Ultramafic rocks are initially cumulates formed during cooling of magmas in hot stagnant-lid settings that feature voluminous volcanism. During

solidification of these cumulates, REE-enriched but HSE-depleted melts interacted with cumulus phases. These cumulates were then variably deformed and/or metamorphosed during tectonic events that either represent (1) shortening, corresponding to volcanic burial, plate-breaking or plate tectonic subduction (panel **a**); or (2) intra-crustal diapirism corresponding to gravitational instability (panel **b**). Later, mostly static (talc/carbonate/serpentine) alterations further modified the petrology and geochemistry.

6. Conclusions

Some ultramafic rocks preserved in or near the Isua supracrustal belt have been interpreted as tectonically emplaced mantle peridotites that require >3.7 Ga onset of plate tectonics (e.g., Nutman et al., 2020; Van de Löcht et al., 2018). In contrast, this study shows that cumulates and mantle rocks may have similar primary rock textures, and whole-rock geochemistry and igneous mineral assemblages generated by olivine-dominated rocks interacting with melts. Differences between Isua and Pilbara ultramafic rocks may largely have resulted from different alterations and/or deformation experienced by these rocks, which are also consistent with crustal conditions (Waterton et al., 2022; Müller et al., in prep.). In contrast, other characteristics of these rocks, such as certain types of spinel geochemistry (e.g., Fe-Ti trends in Cr#-Mg# space; Barnes and Roeder, 2001) as well as cumulate textures, appear to be unique to cumulates. Furthermore, melts that have interacted with Isua and Pilbara ultramafic rocks should be co-genetic melts generated in magma chambers or deep, potentially reduced mantle, which cannot be explained by sub-arc mantle origins. Thus, we conclude that no features preserved in ultramafic rocks of the Isua supracrustal belt and East Pilbara Terrane are diagnostic of plate tectonic-related mantle slices, but instead are compatible with crustal cumulates. Again, it is important to note that these interpretations do not exclude plate tectonic origins for the formation of the Isua supracrustal belt (e.g., Van Kranendonk, 2010; Nutman et al., 2020), but they permit a hot stagnant-lid tectonic origin for this terrane, consistent with recent studies for the belt (Ramírez-Salazar et al., 2021; Webb et al., 2020; Zuo et al., 2021). Therefore, because the East Pilbara Terrane can also be explained in terms of a hot stagnant-lid setting (e.g., Collins et al., 1998; Van Kranendonk et al., 2007), no tectonic shift between the Eoarchean and Paleoarchean is required. Short episodes of local plate tectonic processes during the Eo- and Paleoarchean might be possible, as regional stagnant-lid processes may have coexisted with local plate tectonic processes in early terrestrial planets (e.g., Van Kranendonk, 2010; Yin, 2012a; Yin, 2012b). Nonetheless, our findings show that a ≤3.2 Ga initiation of plate tectonics is viable.

Acknowledgements

We thank An Li for his sampling assistance, Martin Van Kranendonk for field logistics advice, Weiqiang Li and Weihao Yan for assistance in geochemical analyses, and Gary Byerly for insights on igneous textures and petrogenesis. Funding support comes from the American Chemical Society Petroleum Research Fund (PRF-53549-ND8), start-up funds from the University of Hong Kong, and the General Research Fund of the Hong Kong Research Grants Council (#17305718), all to A.A.G.W. Reviewer contributions are gratefully acknowledged. L. A. acknowledges the support of the Czech Science Foundation through the project no. 19-08066S and institutional support RVO67985831 of the Institute of Geology of the Czech Academy of Sciences. Reviewer contributions are gratefully acknowledged.

Data Availability Statement

Datasets for this research can be found in supplementary tables (Table S1 to S3) and references. Figure S1 to S3 can be found in the Supplementary Information file. Datasets generated by this research can also be found at the DataHub repository (https://datahub.hku.hk/) following the link https://doi.org/10.25442/hku.14220047.

References

Abdallah, S. E., S. Ali, and M. A. Obeid (2019), Geochemistry of an Alaskan-type mafic-ultramafic complex in Eastern Desert, Egypt: New insights and constraints on the Neoproterozoic island arc magmatism, *Geoscience Frontiers*, *10*(3), 941-955. https://doi.org/10.1016/j.gsf.2018.04.009

Ackerman, L., R. J. Walker, I. S. Puchtel, L. Pitcher, E. Jelínek, and L. Strnad (2009), Effects of melt percolation on highly siderophile elements and Os isotopes in subcontinental lithospheric mantle: a study of the upper mantle profile beneath Central Europe, *Geochimica Et Cosmochimica Acta*, *73*(8), 2400-2414. https://doi.org/10.1016/j.gca.2009.02.002

Aldanmaz, E., and N. Koprubasi (2006), Platinum-group-element systematics of peridotites from ophiolite complexes of northwest Anatolia, Turkey: implications for mantle metasomatism by melt percolation in a supra-subduction zone environment, *International Geology Review*, *48*(5), 420-442. https://doi.org/10.2747/0020-6814.48.5.420

Appel, P. (1979), Stratabound copper sulfides in a banded iron-formation and in basaltic tuffs in the early Precambrian Isua supracrustal belt, West Greenland, Economic Geology, 74(1), 45-52. https://doi.org/10.2113/gsecongeo.74.1.45

Arai, T., S. Omori, T. Komiya, and S. Maruyama (2015), Intermediate P/T-type regional metamorphism of the Isua Supracrustal Belt, southern west Greenland: The oldest Pacific-type orogenic belt?, *Tectonophysics*, *662*, 22-39. https://doi.org/10.1016/j.tecto.2015.05.020

Arndt, N., Lesher, C., Czamanske, G., 2005. Mantle-derived magmas and magmatic Ni-Cu-(PGE) deposits. https://doi.org/10.5382/AV100.02

Barnes, S.J., Liu, W., 2012. Pt and Pd mobility in hydrothermal fluids: evidence from komatiites and from thermodynamic modelling. Ore Geology Reviews 44, 49-58. https://doi.org/10.1016/j.oregeorev.2011.08.004

Barnes, S. J., and P. L. Roeder (2001), The range of spinel compositions in terrestrial mafic and ultramafic rocks, *Journal of Petrology*, *42*(12), 2279-2302. https://doi.org/10.1093/petrology/42.12.2279

Barnes, S. J., D. R. Mole, M. Le Vaillant, M. J. Campbell, M. R. Verrall, M. P. Roberts, and N. J. Evans (2016), Poikilitic textures, heteradcumulates and zoned orthopyroxenes in the Ntaka Ultramafic Complex, Tanzania: implications for crystallization mechanisms of oikocrysts, *Journal of Petrology*, *57*(6), 1171-1198. https://doi.org/10.1093/petrology/egw036

Bauer, A., J. Reimink, T. Chacko, B. Foley, S. Shirey, and D. J. G. P. L. Pearson (2020), Hafnium isotopes in zircons document the gradual onset of mobile-lid tectonics, *Geochemical Perspectives Letters*, *14*, 1-6. https://doi.org/10.7185/geochemlet.2015

Beall, A., L. Moresi, and C. M. Cooper (2018), Formation of cratonic lithosphere during the initiation of plate tectonics, *Geology*, *46*(6), 487-490. https://doi.org/10.1130/G39943.1

Becker, H., M. Horan, R. Walker, S. Gao, J.-P. Lorand, and R. Rudnick (2006), Highly siderophile element composition of the Earth's primitive upper mantle: constraints from new data on peridotite massifs and xenoliths, *Geochimica Et Cosmochimica Acta*, *70*(17), 4528-4550. https://doi.org/10.1016/j.gca.2006.06.004

Bédard, J. H. (2018), Stagnant lids and mantle overturns: Implications for Archaean tectonics, magmagenesis, crustal growth, mantle evolution, and the start of plate tectonics, *Geoscience Frontiers*, *9*(1), 19-49. https://doi.org/10.1016/j.gsf.2017.01.005

Birck, J. L., M. R. Barman, and F. Capmas (1997), Re-Os isotopic measurements at the femtomole level in natural samples, *Geostandards newsletter*, *21*(1), 19-27. https://doi.org/10.1111/j.1751-908X.1997.tb00528.x

Bland, M. T., and W. B. McKinnon (2016), Mountain building on Io driven by deep faulting, *Nature*, *9*(6), 429-432, doi:10.1038/ngeo2711. https://doi.org/10.1038/ngeo2711

Bockrath, C., C. Ballhaus, and A. Holzheid (2004), Fractionation of the platinum-group elements during mantle melting, *Science*, *305*(5692), 1951-1953. https://doi.org/10.1126/science.1100160

Borghini, G., Rampone, E., 2007. Postcumulus processes in oceanic-type olivine-rich cumulates: the role of trapped melt crystallization versus melt/rock interaction. Contrib Mineral Petr 154, 619-633. https://doi.org/10.1007/s00410-007-0217-5

Boudier, F., G. Ceuleneer, and A. Nicolas (1988), Shear zones, thrusts and related magmatism in the Oman ophiolite: initiation of thrusting on an oceanic ridge, *Tectonophysics*, *151*(1-4), 275-296. https://doi.org/10.1016/0040-1951(88)90249-1

Brandon, A.D., Creaser, R.A., Shirey, S.B., Carlson, R.W., 1996. Osmium recycling in subduction zones. Science 272, 861-863. https://doi.org/10.1126/science.272.5263.861

Brenan, J., N. Bennett, and Z. Zajacz (2016), Experimental Results on Fractionation of the Highly Siderophile Elements (HSE) at Variable Pressures and Temperatures during Planetary and Magmatic Differentiation, *Reviews in Mineralogy and Geochemistry*, *81*, 1-87, https://doi:10.2138/rmg.2016.81.1.

Brown, M., and T. Johnson (2018), Secular change in metamorphism and the onset of global plate tectonics, *American Mineralogist*, *103*(2), 181-196. https://doi.org/10.2138/am-2018-6166

Büchl, A., G. Brügmann, V. G. Batanova, C. Münker, and A. W. Hofmann (2002), Melt percolation monitored by Os isotopes and HSE abundances: a case study from the mantle section of the Troodos Ophiolite, *Earth and Planetary Science Letters*, *204*(3-4), 385-402. https://doi.org/10.1016/S0012-821X(02)00977-9

Byerly, G., D. Lowe, and C. Heubeck (2019), Geologic evolution of the Barberton Greenstone Belt–a unique record of crustal development, surface processes, and early life 3.55 to 3.20 Ga, *Earth's oldest rocks, 2nd edn. Elsevier, Berlin*. https://doi.org/10.1016/B978-0-444-63901-1.00024-1

1214 Cawood, P. A., C. J. Hawkesworth, S. A. Pisarevsky, B. Dhuime, F. A. Capitanio, and O. Nebel
1215 (2018), Geological archive of the onset of plate tectonics, *J Philosophical Transactions of the*
1216 *Royal Society A: Mathematical, Physical Engineering Sciences*, *376*(2132), 20170405.
1217 https://doi.org/10.1098/rsta.2017.0405
1218 Chadwick, B., 1990. The stratigraphy of a sheet of supracrustal rocks within high-grade orthogneisses
1219 and its bearing on Late Archaean structure in southern West Greenland. Journal of the
1220 Geological Society 147, 639-652. https://doi.org/10.1144/gsjgs.147.4.0639

1221 Chen, Y., and Y. Zhang (2009), Clinopyroxene dissolution in basaltic melt, *Geochimica Et*
1222 *Cosmochimica Acta*, *73*(19), 5730-5747. https://doi.org/10.1016/j.gca.2009.06.016

1223 Chen, B.-Y., J.-J. Yu, and S.-J. Liu (2018), Source characteristics and tectonic setting of mafic–
1224 ultramafic intrusions in North Xinjiang, NW China: insights from the petrology and
1225 geochemistry of the Lubei mafic–ultramafic intrusion, *Lithos*, *308*, 329-345.
1226 https://doi.org/10.1016/j.lithos.2018.03.016
1227 Chin, E. J., C.-T. A. Lee, and J. D. Barnes (2014), Thickening, refertilization, and the deep lithosphere
1228 filter in continental arcs: Constraints from major and trace elements and oxygen isotopes,
1229 *Earth and Planetary Science Letters, 397*, 184-200. https://doi.org/10.1016/j.epsl.2014.04.022
1230 Chin, E. J., K. Shimizu, G. M. Bybee, and M. E. Erdman (2018), On the development of the calc-
1231 alkaline and tholeiitic magma series: A deep crustal cumulate perspective, *Earth and*
1232 *Planetary Science Letters*, *482*, 277-287. https://doi.org/10.1016/j.epsl.2017.11.016
1233 Chin, E. J., V. Soustelle, and Y. Liu (2020), An SPO-induced CPO in composite mantle xenoliths
1234 correlated with increasing melt-rock interaction, *Geochimica Et Cosmochimica Acta*, *278*,
1235 199-218. https://doi.org/10.1016/j.gca.2019.10.002
1236 Coggon, J. A., A. Luguet, R. O. Fonseca, J.-P. Lorand, A. Heuser, and P. W. Appel (2015),
1237 Understanding Re–Os systematics and model ages in metamorphosed Archean ultramafic
1238 rocks: a single mineral to whole-rock investigation, *Geochimica Et Cosmochimica Acta*, *167*,
1239 205-240. https://doi.org/10.1016/j.gca.2015.07.025
1240 Cohen, A. S., and F. G. Waters (1996), Separation of osmium from geological materials by solvent
1241 extraction for analysis by thermal ionisation mass spectrometry, *Analytica Chimica Acta*,
1242 *332*(2-3), 269-275. https://doi.org/10.1016/0003-2670(96)00226-7
1243 Collins, W. J., M. J. Van Kranendonk, and C. Teyssier (1998), Partial convective overturn of
1244 Archaean crust in the east Pilbara Craton, Western Australia: driving mechanisms and
1245 tectonic implications, *Journal of Structural Geology*, *20*(9-10), 1405-1424.
1246 https://doi.org/10.1016/S0191-8141(98)00073-X
1247 Condie, K. C., and S. J. Puetz (2019), Time series analysis of mantle cycles Part II: The geologic
1248 record in zircons, large igneous provinces and mantle lithosphere, *Geoscience Frontiers*,
1249 *10*(4), 1327-1336. https://doi.org/10.1016/j.gsf.2019.03.005
1250 Creaser, R., D. Papanastassiou, and G. Wasserburg (1991), Negative thermal ion mass spectrometry
1251 of osmium, rhenium and iridium, *Geochimica Et Cosmochimica Acta*, *55*(1), 397-401.
1252 https://doi.org/10.1016/0016-7037(91)90427-7

1253 Crowley, J., J. Myers, and G. Dunning (2002), Timing and nature of multiple 3700–3600 Ma tectonic
1254 events in intrusive rocks north of the Isua greenstone belt, southern West Greenland,
1255 Geological Society of America Bulletin, 114(10), 1311-1325. https://doi.org/10.1130/0016-
1256 7606(2002)114<1311:TANOMM>2.0.CO;2

1257 Crowley, J. (2003), U–Pb geochronology of 3810–3630 Ma granitoid rocks south of the Isua
1258 greenstone belt, southern West Greenland, Precambrian Research, 126(3-4), 235-257.
1259 https://doi.org/10.1016/S0301-9268(03)00097-4

1260 Day, J. M., D. G. Pearson, and L. J. Hulbert (2013), Highly siderophile element behaviour during
1261 flood basalt genesis and evidence for melts from intrusive chromitite formation in the
1262 Mackenzie large igneous province, Lithos, 182, 242-258
1263 https://doi.org/10.1016/j.lithos.2013.10.011
1264 Deschamps, F., Godard, M., Guillot, S., Hattori, K., 2013. Geochemistry of subduction zone
1265 serpentinites: A review. Lithos 178, 96-127. https://doi.org/10.1016/j.lithos.2013.05.019

Dymek, R. F., J. L. Boak, and S. C. Brothers (1988a), Titanian chondrodite-and titanian clinohumite-bearing metadunite from the 3800 Ma Isua supracrustal belt, West Greenland; chemistry, petrology and origin, *American Mineralogist*, *73*(5-6), 547-558. https://doi.org/10.1093/petrology/29.6.1353

Dymek, R. F., S. C. Brothers, and C. M. Schiffries (1988b), Petrogenesis of Ultramafic Metamorphic Rocks from the 3800-Ma Isua Supracrustal Belt, West Greenland, *Journal of Petrology*, *29*(6), 1353-1397, doi:DOI 10.1093/petrology/29.6.1353. https://doi.org/10.1093/petrology/29.6.1353

El Dien, H. G., S. Arai, L.-S. Doucet, Z.-X. Li, Y. Kil, D. Fougerouse, S. M. Reddy, D. W. Saxey, and M. Hamdy (2019), Cr-spinel records metasomatism not petrogenesis of mantle rocks, *Nature Communications*, *10*(1), 1-12. https://doi.org/10.1038/s41467-019-13117-1

Elthon, D. (1992), Chemical trends in abyssal peridotites: refertilization of depleted suboceanic mantle, *Journal of Geophysical Research: Solid Earth*, *97*(B6), 9015-9025. https://doi.org/10.1029/92JB00723

Fiorentini, M. L., S. J. Barnes, C. M. Lesher, G. J. Heggie, R. R. Keays, and O. M. Burnham (2010), Platinum group element geochemistry of mineralized and nonmineralized komatiites and basalts, Economic Geology, 105(4), 795-823. https://doi.org/10.2113/gsecongeo.105.4.795

Fiorentini, M. L., S. J. Barnes, W. D. Maier, O. M. Burnham, and G. Heggie (2011), Global variability in the platinum-group element contents of komatiites, Journal of Petrology, 52(1), 83-112. https://doi.org/10.1093/petrology/egq074

Foley, B. J., D. Bercovici, and L. T. Elkins-Tanton (2014), Initiation of plate tectonics from post-magma ocean thermochemical convection, *Journal of Geophysical Research: Solid Earth*, *119*(11), 8538-8561, doi:10.1002/2014JB011121. https://doi.org/10.1002/2014JB011121

François, C., P. Philippot, P. Rey, and D. Rubatto (2014), Burial and exhumation during Archean sagduction in the East Pilbara granite-greenstone terrane, *Earth and Planetary Science Letters*, *396*, 235-251. https://doi.org/10.1016/j.epsl.2014.04.025

Friend, C. R. L., and A. P. Nutman (2011), Dunites from Isua, Greenland: A ca. 3720 Ma window into subcrustal metasomatism of depleted mantle, *Geology*, *39*(7), 663-666, doi:10.1130/G31904.1. https://doi.org/10.1130/G31904.1

Friend, C. R. L., V. C. Bennett, and A. P. Nutman (2002), Abyssal peridotites > 3,800 Ma from southern West Greenland: field relationships, petrography, geochronology, whole-rock and mineral chemistry of dunite and harzburgite inclusions in the Itsaq Gneiss Complex, *Contributions to Mineralogy and Petrology*, *143*(1), 71-92, doi:10.1007/s00410-001-0332-7. https://doi.org/10.1007/s00410-001-0332-7

Gale, A., C. A. Dalton, C. H. Langmuir, Y. J. Su, and J. G. Schilling (2013), The mean composition of ocean ridge basalts, *Geochemistry Geophysics Geosystems*, *14*(3), 489-518, doi:10.1029/2012gc004334. https://doi.org/10.1029/2012GC004334

Garuti, G., E. V. Pushkarev, F. Zaccarini, R. Cabella, and E. Anikina (2003), Chromite composition and platinum-group mineral assemblage in the Uktus Uralian-Alaskan-type complex (Central Urals, Russia), *Mineralium Deposita*, *38*(3), 312-326. https://doi.org/10.1007/s00126-003-0348-1

Gannoun, A., K. W. Burton, J. M. Day, J. Harvey, P. Schiano, and I. Parkinson (2016), Highly siderophile element and Os isotope systematics of volcanic rocks at divergent and convergent plate boundaries and in intraplate settings, *Reviews in Mineralogy and Geochemistry*, *81*(1), 651-724. https://doi.org/10.2138/rmg.2016.81.11

Geological Survey of Western Australia 2013 database, (2013). 1:100 000 GIS Pilbara 2013 update / Geological Survey of Western Australia, in: Western Australia. Department of, M., Petroleum, Exploration Incentive, S. (Eds.). Geological Survey of Western Australia, East Perth, Western Australia ©2013.

Goodrich, C. A., A. M. Fioretti, M. Tribaudino, and G. Molin (2001), Primary trapped melt inclusions in olivine in the olivine-augite-orthopyroxene ureilite Hughes 009, *Geochimica Et Cosmochimica Acta*, *65*(4), 621-652. https://doi.org/10.1016/S0016-7037(00)00521-4

Gordeychik, B., T. Churikova, A. Kronz, C. Sundermeyer, A. Simakin, and G. Wörner (2018), Growth of, and diffusion in, olivine in ultra-fast ascending basalt magmas from Shiveluch volcano, *Scientific reports*, *8*(1), 1-15. https://doi.org/10.1038/s41598-018-30133-1

Guice, G., McDonald, I., Hughes, H., Schlatter, D., Goodenough, K., MacDonald, J., Faithfull, J., 2018. Assessing the validity of negative high field strength-element anomalies as a proxy for Archaean subduction: evidence from the Ben Strome Complex, NW Scotland. Geosciences 8, 338. https://doi.org/10.3390/geosciences8090338

Guotana, J. M., T. Morishita, I. Nishio, A. Tamura, T. Mizukami, K. Tani, Y. Harigane, K. Szilas, and D. G. Pearson (2022), Deserpentinization and high-pressure (eclogite-facies) metamorphic features in the Eoarchean ultramafic body from Isua, Greenland, Geoscience Frontiers, 101298. https://doi.org/10.1016/j.gsf.2021.101298

Hanghøj, K., P. B. Kelemen, D. Hassler, and M. Godard (2010), Composition and Genesis of Depleted Mantle Peridotites from the Wadi Tayin Massif, Oman Ophiolite; Major and Trace Element Geochemistry, and Os Isotope and PGE Systematics, *Journal of Petrology*, *51*(1-2), 201-227. https://doi.org/10.1093/petrology/egp077

Hansen, V. (2007), Subduction origin on early Earth: A hypothesis, *Geology*, *35*(12), 1059-1062. https://doi.org/10.1130/G24202A.1

Harrison, T. M. (2009), The Hadean Crust: Evidence from > 4 Ga Zircons, *Annual Review of Earth and Planetary Sciences*, *37*, 479-505. https://doi.org/10.1146/annurev.earth.031208.100151

Hickman, A. H. (2021), EAST PILBARA CRATON: A RECORD OF ONE BILLION YEARS IN THE GROWTH OF ARCHEAN CONTINENTAL CRUST, *Geological Survey of Western Australia, Report 143*, 1-187.

Himmelberg, G. R., and R. A. Loney (1995), *Characteristics and petrogenesis of Alaskan-type ultramafic-mafic intrusions, southeastern Alaska*, US Government Printing Office. https://doi.org/10.3133/pp1564

Holtzman, B. K., D. L. Kohlstedt, M. E. Zimmerman, F. Heidelbach, T. Hiraga, and J. Hustoft (2003), Melt segregation and strain partitioning: Implications for seismic anisotropy and mantle flow, *Science*, *301*(5637), 1227-1230. https://doi.org/10.1126/science.1087132

Hopkins, M., T. M. Harrison, and C. E. Manning (2008), Low heat flow inferred from> 4 Gyr zircons suggests Hadean plate boundary interactions, *Nature*, *456*(7221), 493-496. https://doi.org/10.1038/nature07465

Hunter, R. (1996), Texture development in cumulate rocks, in *Developments in Petrology*, edited, pp. 77-101, Elsevier. https://doi.org/10.1016/S0167-2894(96)80005-4

Ionov, D. A. (2010), Petrology of mantle wedge lithosphere: new data on supra-subduction zone peridotite xenoliths from the andesitic Avacha volcano, Kamchatka, *Journal of Petrology*, *51*(1-2), 327-361. https://doi.org/10.1093/petrology/egp090

Jagoutz, E., Palme, H., Baddenhausen, H., Blum, K., Cendales, M., Dreibus, G., Spettel, B., Lorenz, V., Wänke, H., 1979. The abundances of major, minor and trace elements in the earth's mantle as derived from primitive ultramafic nodules, Lunar and Planetary Science Conference Proceedings, pp. 2031-2050.

Janoušek, V., C. M. Farrow, and V. Erban (2006), Interpretation of whole-rock geochemical data in igneous geochemistry: Introducing Geochemical Data Toolkit (GCDkit), *Journal of Petrology*, *47*(6), 1255-1259. https://doi.org/10.1093/petrology/egl013

Johannsen, A. (1931), *A Descriptive Petrography of the Igneous Rocks: Introduction, textures, classifications and glossary*, University of Chicago Press.

Johnson, D., P. Hooper, and R. Conrey (1999), XRF Method XRF Analysis of Rocks and Minerals for Major and Trace Elements on a Single Low Dilution Li-Tetraborate Fused Bead, *Adv. X-ray anal*, *41*, 843-867.

Johnson, T. E., M. Brown, B. J. P. Kaus, and J. A. VanTongeren (2014), Delamination and recycling of Archaean crust caused by gravitational instabilities, Nature Geoscience, 7(1), 47-52, doi:10.1038/Ngeo2019. https://doi.org/10.1038/ngeo2019

Johnson, T. E., M. Brown, N. J. Gardiner, C. L. Kirkland, and R. H. Smithies (2017), Earth's first stable continents did not form by subduction, *Nature*, *543*(7644), 239-+. https://doi.org/10.1038/nature21383

Kaczmarek, M. A., S. M. Reddy, A. P. Nutman, C. R. L. Friend, and V. C. Bennett (2016), Earth's oldest mantle fabrics indicate Eoarchaean subduction, *Nature Communications*, *7*. https://doi.org/10.1038/ncomms10665

Kelemen, P. B. (1990), Reaction between ultramafic rock and fractionating basaltic magma I. Phase relations, the origin of calc-alkaline magma series, and the formation of discordant dunite, *Journal of Petrology*, *31*(1), 51-98. https://doi.org/10.1093/petrology/31.1.51

Kelemen, P. B., H. J. Dick, and J. E. Quick (1992), Formation of harzburgite by pervasive melt/rock reaction in the upper mantle, *Nature, 358(6388)*, 635-641. https://doi.org/10.1038/358635a0

Keppler, H. (1996), Constraints from partitioning experiments on the composition of subduction-zone fluids, Nature, 380(6571), 237-240. https://doi.org/10.1038/380237a0

Khatun, S., S. K. Mondal, M.-F. Zhou, V. Balaram, and H. M. Prichard (2014), Platinum-group element (PGE) geochemistry of Mesoarchean ultramafic–mafic cumulate rocks and chromitites from the Nuasahi Massif, Singhbhum Craton (India), *Lithos*, *205*, 322-340. https://doi.org/10.1016/j.lithos.2014.07.013

Khedr, M. Z., S. Arai, M. Python, and A. Tamura (2014), Chemical variations of abyssal peridotites in the central Oman ophiolite: evidence of oceanic mantle heterogeneity, *Gondwana Research*, *25*(3), 1242-1262. https://doi.org/10.1016/j.gr.2013.05.010

Kirkland, C., M. Hartnady, M. Barham, H. Olierook, A. Steenfelt, and J. Hollis (2021), Widespread reworking of Hadean-to-Eoarchean continents during Earth's thermal peak, *Nature Communications*, *12*(1), 1-9. https://doi.org/10.1038/s41467-020-20514-4

Knaack, C., S. Cornelius, and P. Hooper (1994), Trace element analyses of rocks and minerals by ICP-MS, *Geoanalytical Laboratory. Wash. State Univ*, *2*, 18.

Korenaga, J. (2011), Thermal evolution with a hydrating mantle and the initiation of plate tectonics in the early Earth, *Journal of Geophysical Research: Solid Earth*, *116*(B12). https://doi.org/10.1029/2011JB008410

Krause, J., G. Brügmann, and E. Pushkarev (2011), Chemical composition of spinel from Uralian-Alaskan-type Mafic–Ultramafic complexes and its petrogenetic significance, *Contributions to Mineralogy and Petrology 161*(2), 255-273. https://doi.org/10.1007/s00410-010-0530-2

Kusky, T., Windley, B.F., Polat, A., Wang, L., Ning, W., Zhong, Y., 2021. Archean dome-and-basin style structures form during growth and death of intraoceanic and continental margin arcs in accretionary orogens. Earth-Science Reviews 220, 103725. https://doi.org/10.1016/j.earscirev.2021.103725

Lenardic, A. (2018), The diversity of tectonic modes and thoughts about transitions between them, *Philosophical Transactions of the Royal Society A: Mathematical, Physical and Engineering Sciences*, *376*(2132), 20170416. https://doi.org/10.1098/rsta.2017.0416

Lesher, C. M., O. M. Burnham, R. R. Keays, S. J. Barnes, and L. Hulbert (2001), Trace-element geochemistry and petrogenesis of barren and ore-associated komatiites, The Canadian Mineralogist, 39(2), 673-696. https://doi.org/10.2113/gscanmin.39.2.673

Lightfoot, P. C., and R. R. Keays (2005), Siderophile and chalcophile metal variations in flood basalts from the Siberian trap, Noril'sk region: Implications for the origin of the Ni-Cu-PGE sulfide ores, Economic Geology, 100(3), 439-462. https://doi.org/10.2113/gsecongeo.100.3.439

Lundeen, M. T. (1978), Emplacement of the Ronda peridotite, Sierra Bermeja, Spain, *Geological Society of America Bulletin*, *89*(2), 172-180. https://doi.org/10.1130/0016-7606(1978)89<172:EOTRPS>2.0.CO;2

Maier, W. D., F. Roelofse, and S.-J. Barnes (2003), The concentration of the platinum-group elements in South African komatiites: implications for mantle sources, melting regime and PGE fractionation during crystallization, *Journal of Petrology*, *44*(10), 1787-1804. https://doi.org/10.1093/petrology/egg059

Mallik, A., S. Lambart, and E. J. Chin (2020), Tracking the evolution of magmas from heterogeneous mantle sources to eruption, in *Mantle Convection and Surface Expressions*, edited, AGU Monograph Series. https://arxiv.org/abs/2001.00928

Malvoisin, B., 2015. Mass transfer in the oceanic lithosphere: Serpentinization is not isochemical. Earth Planet Sc Lett 430, 75-85. https://doi.org/10.1016/j.epsl.2015.07.043

Marchi, S., Bottke, W., Elkins-Tanton, L., Bierhaus, M., Wuennemann, K., Morbidelli, A., Kring, D., 2014. Widespread mixing and burial of Earth's Hadean crust by asteroid impacts. Nature 511, 578-582. https://doi.org/10.1038/nature13539

Marchesi, C., Garrido, C. J., Proenza, J. A., Hidas, K., Varas-Reus, M. I., Butjosa, L., and Lewis, J. F., 2016, Geochemical record of subduction initiation in the sub-arc mantle: Insights from the Loma Caribe peridotite (Dominican Republic): Lithos, v. 252, p. 1-15. https://doi.org/10.1016/j.lithos.2016.02.009

McDonough, W. F., and S. S. Sun (1995), The Composition of the Earth, *Chemical Geology*, *120*(3-4), 223-253, doi:Doi 10.1016/0009-2541(94)00140-4. https://doi.org/10.1016/0009-2541(94)00140-4

McIntyre, T., D. Pearson, K. Szilas, and T. Morishita (2019), Implications for the origins of Eoarchean ultramafic rocks of the North Atlantic Craton: a study of the Tussaap Ultramafic complex, Itsaq Gneiss complex, southern West Greenland, *Contributions to Mineralogy and Petrology*, *174*(12), 1-21. https://doi.org/10.1007/s00410-019-1628-9

Moore, W. B., J. I. Simon, and A. A. G. Webb (2017), Heat-pipe planets, *Earth and Planetary Science Letters*, *474*, 13-19. https://doi.org/10.1016/j.epsl.2017.06.015

Moore, W. B., and A. A. G. Webb (2013), Heat-pipe Earth, *Nature*, *501*(7468), 501-505. https://doi.org/10.1038/nature12473

Müller T., Sorger D., Zuo J., Webb A.A.G., Ramirez-Salazar A., Piazolo S. (In preparation): Earth's earliest phaneritic ultramafic rocks 2: Exploring the role of CO_2 in evaluating metamorphic conditions.

Münker, C., 1998. Nb/Ta fractionation in a Cambrian arc/back arc system, New Zealand: source constraints and application of refined ICPMS techniques. Chem Geol 144, 23-45. https://doi.org/10.1016/S0009-2541(97)00105-8

Nagaya, T., S. R. Wallis, H. Kobayashi, K. Michibayashi, T. Mizukami, Y. Seto, A. Miyake, and M. Matsumoto (2014), Dehydration breakdown of antigorite and the formation of B-type olivine CPO, *Earth and Planetary Science Letters*, *387*, 67-76. https://doi.org/10.1016/j.epsl.2013.11.025

Nagaya, T., Wallis, S.R., Seto, Y., Miyake, A., Soda, Y., Uehara, S., Matsumoto, M., 2017. Minimizing and quantifying mis-indexing in electron backscatter diffraction (EBSD) determinations of antigorite crystal directions. J Struct Geol 95, 127-141. https://doi.org/10.1016/j.jsg.2016.12.006

Nagel, T.J., Hoffmann, J.E., Münker, C., 2012. Generation of Eoarchean tonalite-trondhjemite-granodiorite series from thickened mafic arc crust. Geology 40, 375-378. https://doi.org/10.1130/G32729.1

Næraa, T., A. Schersten, M. T. Rosing, A. I. S. Kemp, J. E. Hoffmann, T. F. Kokfelt, and M. J. Whitehouse (2012), Hafnium isotope evidence for a transition in the dynamics of continental growth 3.2Gyr ago, *Nature*, *485*(7400), 627-+. https://doi.org/10.1038/nature11140

Niu, Y.L., Hekinian, R., 1997. Basaltic liquids and harzburgitic residues in the Garrett Transform: A case study at fast-spreading ridges. Earth Planet Sc Lett 146, 243-258. https://doi.org/10.1016/S0012-821X(96)00218-X

Niu, Y. L. (2004), Bulk-rock major and trace element compositions of abyssal peridotites: Implications for mantle melting, melt extraction and post-melting processes beneath mid-ocean ridges, *Journal of Petrology*, *45*(12), 2423-2458. https://doi.org/10.1016/S0012-821X(96)00218-X

Nutman, A. P., and C. R. L. Friend (2009), New 1:20,000 scale geological maps, synthesis and history of investigation of the Isua supracrustal belt and adjacent orthogneisses, southern West

Greenland: A glimpse of Eoarchaean crust formation and orogeny, *Precambrian Research*, *172*(3-4), 189-211. https://doi.org/10.1016/j.precamres.2009.03.017
Nutman, A.P., 1986. The early Archaean to Proterozoic history of the Isukasia area, southern West Greenland. Bulletin Gronlands Geologiske Undersogelse 154. https://doi.org/10.34194/bullggu.v154.6696
Nutman, A. P., V. R. McGregor, C. R. L. Friend, V. C. Bennett, and P. D. Kinny (1996), The Itsaq Gneiss Complex of southern west Greenland; The world's most extensive record of early crustal evolution (3900-3600 Ma), *Precambrian Research*, *78*(1-3), 1-39. https://doi.org/10.1016/0301-9268(95)00066-6
Nutman, A.P., Friend, C.R.L., Bennett, V.C., 2002. Evidence for 3650-3600 Ma assembly of the northern end of the Itsaq Gneiss Complex, Greenland: Implication for early Archaean tectonics. Tectonics 21. https://doi.org/10.1029/2000TC001203
Nutman, A.P., Friend, C.R., Bennett, V.C., Wright, D., Norman, M.D., 2010. ⩾ 3700 Ma pre-metamorphic dolomite formed by microbial mediation in the Isua supracrustal belt (W. Greenland): simple evidence for early life? Precambrian Res 183, 725-737. https://doi.org/10.1016/j.precamres.2010.08.006
Nutman, A. P., V. C. Bennett, and C. R. Friend (2013a), The emergence of the Eoarchaean proto-arc: evolution of a c. 3700 Ma convergent plate boundary at Isua, southern West Greenland, *Geological Society, London, Special Publications*, *389*, SP389. 385. https://doi.org/10.1144/SP389.5
Nutman, A. P., V. C. Bennett, C. R. L. Friend, H. Hidaka, K. Yi, S. R. Lee, and T. Kamiichi (2013b), THE ITSAQ GNEISS COMPLEX OF GREENLAND: EPISODIC 3900 TO 3660 Ma JUVENILE CRUST FORMATION AND RECYCLING IN THE 3660 TO 3600 Ma ISUKASIAN OROGENY, *American Journal of Science*, *313*(9), 877-911. https://doi.org/10.2475/09.2013.03
Nutman, A.P., Bennett, V.C., Friend, C.R., Yi, K., Lee, S.R., 2015. Mesoarchaean collision of Kapisilik terrane 3070 Ma juvenile arc rocks and> 3600 Ma Isukasia terrane continental crust (Greenland). Precambrian Res 258, 146-160. https://doi.org/10.1016/j.precamres.2014.12.013
Nutman, A. P., V. C. Bennett, C. R. Friend, and K. Yi (2020), Eoarchean contrasting ultra-high-pressure to low-pressure metamorphisms (< 250 to> 1000° C/GPa) explained by tectonic plate convergence in deep time, *Precambrian Research*, 105770. https://doi.org/10.1016/j.precamres.2020.105770
Nutman, A. P., M. R. Scicchitano, C. R. Friend, V. C. Bennett, and A. R. Chivas (2021a), Isua (Greenland)~ 3700 Ma meta-serpentinite olivine Mg# and δ18O signatures show connection between the early mantle and hydrosphere: Geodynamic implications, *Precambrian Research*, 361, 106249. https://doi.org/10.1016/j.precamres.2021.106249
Nutman, A.P., Bennett, V.C., Friend, C.R.L., Polat, A., Hoffmann, E., Van Kranendonk, M., 2021b. Fifty years of the Eoarchean and the case for evolving uniformitarianism. Precambrian Res 367, 106442. https://doi.org/10.1016/j.precamres.2021.106442
O'Neill, C., and V. Debaille (2014), The evolution of Hadean–Eoarchaean geodynamics, *Earth and Planetary Science Letters*, *406*, 49-58. https://doi.org/10.1016/j.epsl.2014.08.034
O'NEILL, H. S. C., and J. A. MAVROGENES (2002), The Sulfide Capacity and the Sulfur Content at Sulfide Saturation of Silicate Melts at 1400°C and 1 bar, *Journal of Petrology*, *43*(6), 1049-1087, doi:10.1093/petrology/43.6.1049. https://doi.org/10.1093/petrology/43.6.1049
O'Reilly, T. C., and G. F. Davies (1981), Magma transport of heat on Io: A mechanism allowing a thick lithosphere, *Geophysical Research Letters*, *8*(4), 313-316. https://doi.org/10.1029/GL008i004p00313
Parkinson, I. J., and J. A. Pearce (1998), Peridotites from the Izu–Bonin–Mariana forearc (ODP Leg 125): evidence for mantle melting and melt–mantle interaction in a supra-subduction zone setting, *Journal of Petrology*, *39*(9), 1577-1618. https://doi.org/10.1093/petroj/39.9.1577
Paulick, H., W. Bach, M. Godard, J. C. M. De Hoog, G. Suhr, and J. Harvey (2006), Geochemistry of abyssal peridotites (Mid-Atlantic Ridge, 15 degrees 20 ' N, ODP Leg 209): Implications for fluid/rock interaction in slow spreading environments, *Chemical Geology*, *234*(3-4), 179-210 https://doi.org/10.1016/j.chemgeo.2006.04.011

Pearce, J. A., and M. K. Reagan (2019), Identification, classification, and interpretation of boninites from Anthropocene to Eoarchean using Si-Mg-Ti systematics, *Geosphere*, *15*(4), 1008-1037. https://doi.org/10.1130/GES01661.1

Polat, A., and A. W. Hofmann (2003), Alteration and geochemical patterns in the 3.7-3.8 Ga Isua greenstone belt, West Greenland, *Precambrian Research*, *126*(3-4), 197-218. https://doi.org/10.1016/S0301-9268(03)00095-0

Ramírez-Salazar, A., T. Müller, S. Piazolo, A. A. G. Webb, C. Hauzenberger, J. Zuo, P. Haproff, J. Harvey, T. K. Wong, and C. Charlton (2021), Tectonics of the Isua supracrustal belt 1: P-T-X-d constraints of a poly-metamorphic terrane, *Tectonics*, *40*(3), e2020TC006516. https://doi.org/10.1029/2020tc006516

Reimink, J. R., J. H. Davies, A. M. Bauer, and T. Chacko (2020), A comparison between zircons from the Acasta Gneiss Complex and the Jack Hills region, *Earth and Planetary Science Letters*, *531*, 115975. https://doi.org/10.1016/j.epsl.2019.115975

Shen, T., J. Hermann, L. Zhang, Z. Lü, J. A. Padrón-Navarta, B. Xia, and T. Bader (2015), UHP metamorphism documented in Ti-chondrodite-and Ti-clinohumite-bearing serpentinized ultramafic rocks from Chinese southwestern Tianshan, *Journal of Petrology*, *56*(7), 1425-1458. https://doi.org/10.1093/petrology/egv042

Shirey, S. B., and R. J. Walker (1995), Carius tube digestion for low-blank rhenium-osmium analysis, *Analytical Chemistry*, *67*(13), 2136-2141. https://doi.org/10.1021/ac00109a036

Shirey, S. B., and R. J. Walker (1998), The Re-Os isotope system in cosmochemistry and high-temperature geochemistry, *Annual Review of Earth and Planetary Sciences*, *26*(1), 423-500. https://doi.org/10.1146/annurev.earth.26.1.423

Smart, K.A., Tappe, S., Stern, R.A., Webb, S.J., Ashwal, L.D., 2016. Early Archaean tectonics and mantle redox recorded in Witwatersrand diamonds. Nat Geosci 9, 255-259. https://doi.org/10.1038/ngeo2628

Smithies, R., D. Champion, M. Van Kranendonk, and A. Hickman (2007), Geochemistry of volcanic rocks of the northern Pilbara Craton, Western Australia, *Geological Survey of Western Australia Report*, *104*.

Smithies, R., Champion, D., Van Kranendonk, M., 2009. Formation of Paleoarchean continental crust through infracrustal melting of enriched basalt. Earth Planet Sc Lett 281, 298-306. https://doi.org/10.1016/j.epsl.2009.03.003

Smithies, R. H., Y. Lu, C. L. Kirkland, T. E. Johnson, D. R. Mole, D. C. Champion, L. Martin, H. Jeon, M. T. Wingate, and S. P. Johnson (2021), Oxygen isotopes trace the origins of Earth's earliest continental crust, *Nature*, *592*(7852), 70-75. https://doi.org/10.1038/s41586-021-03337-1

Standish, J., S. Hart, J. Blusztajn, H. Dick, and K. Lee (2002), Abyssal peridotite osmium isotopic compositions from cr-spinel, *Geochemistry, Geophysics, Geosystems*, *3*(1), 1-24. https://doi.org/10.1029/2001GC000161

Stern, R. J. (2008), Modern-style plate tectonics began in Neoproterozoic time: An alternative interpretation of Earth's tectonic history, *When did plate tectonics begin on planet Earth*, *265*, 280. https://doi.org/10.1130/2008.2440(13)

Stern, R. J., T. Gerya, and P. J. Tackley (2017), Stagnant lid tectonics: Perspectives from silicate planets, dwarf planets, large moons, and large asteroids, *Geoscience Frontiers*, *9*(1). https://doi.org/10.1016/j.gsf.2017.06.004

Szilas, K., V. J. Van Hinsberg, R. A. Creaser, and A. F. M. Kisters (2014), The geochemical composition of serpentinites in the Mesoarchaean Tartoq Group, SW Greenland: Harzburgitic cumulates or melt-modified mantle?, *Lithos*, *198*, 103-116. https://doi.org/10.1016/j.lithos.2014.03.024

Szilas, K., P. B. Kelemen, and M. T. Rosing (2015), The petrogenesis of ultramafic rocks in the > 3.7 Ga Isua supracrustal belt, southern West Greenland: Geochemical evidence for two distinct magmatic cumulate trends, *Gondwana Research*, *28*(2), 565-580. https://doi.org/10.1016/j.gr.2014.07.010

Szilas, K., V. van Hinsberg, I. McDonald, T. Næraa, H. Rollinson, J. Adetunji, and D. Bird (2018), Highly refractory Archaean peridotite cumulates: Petrology and geochemistry of the Seqi Ultramafic Complex, SW Greenland, *Geoscience Frontiers*, *9*(3), 689-714. https://doi.org/10.1016/j.gsf.2017.05.003

Tamura, A., and S. Arai (2006), Harzburgite-dunite-orthopyroxenite suite as a record of supra-subduction zone setting for the Oman ophiolite mantle, *Lithos*, *90*(1-2), 43-56. https://doi.org/10.1016/j.lithos.2005.12.012

Tang, C., A. Webb, W. Moore, Y. Wang, T. Ma, and T. Chen (2020), Breaking Earth's shell into a global plate network, *Nature Communications*, *11*(1), 1-6. https://doi.org/10.1038/s41467-020-17480-2

Thakurta, J., E. M. Ripley, and C. Li (2008), Geochemical constraints on the origin of sulfide mineralization in the Duke Island Complex, southeastern Alaska, *Geochemistry, Geophysics, Geosystems*, *9*(7). https://doi.org/10.1029/2008GC001982

Topuz, G., E. Hegner, S. M. Homam, L. Ackerman, J. A. Pfänder, and H. Karimi (2018), Geochemical and geochronological evidence for a Middle Permian oceanic plateau fragment in the Paleo-Tethyan suture zone of NE Iran, Contributions to Mineralogy and Petrology, 173(10), 81. https://doi.org/10.1007/s00410-018-1506-x

Van de Löcht, J., J. Hoffmann, C. Li, Z. Wang, H. Becker, M. T. Rosing, R. Kleinschrodt, and C. Münker (2018), Earth's oldest mantle peridotites show entire record of late accretion, *Geology*, *46*(3), 199-202. https://doi.org/10.1130/G39709.1

Van de Löcht, J., J. Hoffmann, M. Rosing, P. Sprung, and C. Münker (2020), Preservation of Eoarchean mantle processes in~ 3.8 Ga peridotite enclaves in the Itsaq Gneiss Complex, southern West Greenland, *Geochimica Et Cosmochimica Acta*, *280*, 1-25. https://doi.org/10.1016/j.gca.2020.03.043

Van Kranendonk, M. J. (2010), Two Types of Archean Continental Crust: Plume and Plate Tectonics on Early Earth, *American Journal of Science*, *310*(10), 1187-1209. https://doi.org/10.2475/10.2010.01

Van Kranendonk, M. J., W. J. Collins, A. Hickman, and M. J. Pawley (2004), Critical tests of vertical vs. horizontal tectonic models for the Archaean East Pilbara Granite-Greenstone Terrane, Pilbara Craton, Western Australia, *Precambrian Research*, *131*(3-4), 173-211. https://doi.org/10.1016/j.precamres.2003.12.015

Van Kranendonk, M. J., R. H. Smithies, A. H. Hickman, and D. C. Champion (2007), Review: secular tectonic evolution of Archean continental crust: interplay between horizontal and vertical processes in the formation of the Pilbara Craton, Australia, *Terra Nova*, *19*(1), 1-38. https://doi.org/10.1111/j.1365-3121.2006.00723.x

Völkening, J., T. Walczyk, and K. G. Heumann (1991), Osmium isotope ratio determinations by negative thermal ionization mass spectrometry, *International Journal of Mass Spectrometry and Ion Processes*, *105*(2), 147-159. https://doi.org/10.1016/0168-1176(91)80077-Z

Wager, L. R., and G. M. Brown (1967), *Layered igneous rocks*, WH Freeman.

Wal, D. V. d., and R. L. Vissers (1993), Uplift and emplacement of upper mantle rocks in the western Mediterranean, *Geology*, *21*(12), 1119-1122. https://doi.org/10.1130/0091-7613(1993)021<1119:UAEOUM>2.3.CO;2

Wang, Z., H. Becker, and T. Gawronski (2013), Partial re-equilibration of highly siderophile elements and the chalcogens in the mantle: A case study on the Baldissero and Balmuccia peridotite massifs (Ivrea Zone, Italian Alps), *Geochimica Et Cosmochimica Acta*, *108*, 21-44. https://doi.org/10.1016/j.gca.2013.01.021

Waterton, P., Mungall, J., Pearson, D.G., 2021. The komatiite-mantle platinum-group element paradox. Geochim Cosmochim Ac 313, 214-242. https://doi.org/10.1016/j.gca.2021.07.037

Waterton, P., J. M. Guotana, I. Nishio, T. Morishita, K. Tani, S. Woodland, H. Legros, D. G. Pearson, and K. Szilas (2022), No mantle residues in the Isua Supracrustal Belt, Earth and Planetary Science Letters, 579, 117348, https://doi.org/10.1016/j.epsl.2021.117348.

Webb, A. A. G., T. Müller, J. Zuo, P. J. Haproff, and A. Ramírez-Salazar (2020), A non–plate tectonic model for the Eoarchean Isua supracrustal belt, *Lithosphere*, *12*(1), 166-179. https://doi.org/10.1130/L1130.1

Wiemer, D., C. Schrank, D. Murphy, L. Wenham, and C. Allen (2018), Earth's oldest stable crust in the Pilbara Craton formed by cyclic gravitational overturns, *Nature Geoscience*, *11*(5), 357-361, doi:10.1038/s41561-018-0105-9. https://doi.org/10.1038/s41561-018-0105-9

Williams, I. R. (1999), Geology of the Muccan 1:100 000 sheet, Geological Survey of Western Australia.

Wooden, J.L., Czamanske, G.K., Fedorenko, V.A., Arndt, N.T., Chauvel, C., Bouse, R.M., King, B.-S.W., Knight, R.J., Siems, D.F., 1993. Isotopic and trace-element constraints on mantle and crustal contributions to Siberian continental flood basalts, Noril'sk area, Siberia. Geochim Cosmochim Ac 57, 3677-3704. https://doi.org/10.1016/0016-7037(93)90149-Q

Yao, Z., K. Qin, Q. Wang, and S. Xue (2019), Weak B-Type Olivine Fabric Induced by Fast Compaction of Crystal Mush in a Crustal Magma Reservoir, *Journal of Geophysical Research: Solid Earth*. https://doi.org/10.1029/2018JB016728

Yin, A. (2012a), An episodic slab-rollback model for the origin of the Tharsis rise on Mars: Implications for initiation of local plate subduction and final unification of a kinematically linked global plate-tectonic network on Earth, *Lithosphere*, *4*(6), 553-593. https://doi.org/10.1130/L195.1

Yin, A. (2012b), Structural analysis of the Valles Marineris fault zone: Possible evidence for large-scale strike-slip faulting on Mars, *Lithosphere*, *4*(4), 286-330. https://doi.org/10.1130/L192.1

Zuo, J., A. A. G. Webb, S. Piazolo, Q. Wang, T. Müller, A. Ramírez-Salazar, and P. J. Haproff (2021), Tectonics of the Isua Supracrustal Belt 2: Microstructures Reveal Distributed Strain in the Absence of Major Fault Structures, *Tectonics*, *40*(3), e2020TC006514. https://doi.org/10.1029/2020tc006514